Doping dependence of spin and orbital correlations in layered manganites

Maria Daghofer
Institute of Theoretical and Computational Physics, Graz University of Technology, Petersgasse 16, A-8010 Graz, Austria and Max-Planck-Institut für Festkörperforschung, Heisenbergstrasse 1, D-70569 Stuttgart, Germany

Andrzej M. Oleś
Marian Smoluchowski Institute of Physics, Jagellonian University, Reymonta 4, PL-30059 Kraków, Poland, and Max-Planck-Institut für Festkörperforschung, Heisenbergstrasse 1, D-70569 Stuttgart, Germany

Danilo R. Neuber and Wolfgang von der Linden
Institute of Theoretical and Computational Physics, Graz University of Technology, Petersgasse 16, A-8010 Graz, Austria
(Received 6 January 2006; revised manuscript received 24 February 2006; published 31 March 2006)

We investigate the interplay between spin and orbital correlations in monolayer and bilayer manganites using an effective spin-orbital *t-J* model which treats explicitly the e_g orbital degrees of freedom coupled to classical t_{2g} spins. Using finite clusters with periodic boundary conditions, the orbital many-body problem is solved by exact diagonalization, either by optimizing spin configuration at zero temperature or by using classical Monte Carlo simulations for the spin subsystem at finite temperature. In undoped two-dimensional clusters, a complementary behavior of orbital and spin correlations is found—the ferromagnetic spin order coexists with alternating orbital order, while the antiferromagnetic spin order, triggered by t_{2g} spin superexchange, coexists with ferro orbital order. With a finite crystal-field term, we introduce a realistic model for $La_{1-x}Sr_{1+x}MnO_4$, describing a gradual change from predominantly out-of-plane $3z^2-r^2$ to in-plane x^2-y^2 orbital occupation under increasing doping. The present electronic model is sufficient to explain the stability of the CE phase in monolayer manganites at doping $x=0.5$ and also yields the *C*-type antiferromagnetic phase found in $Nd_{1-x}Sr_{1+x}MnO_4$ at high doping. Also in bilayer manganites magnetic phases and the accompanying orbital order change with increasing doping. Here the model predicts *C*-AF and *G*-AF phases at high doping $x>0.75$, as found experimentally in $La_{2-2x}Sr_{1+2x}Mn_2O_7$.

DOI: 10.1103/PhysRevB.73.104451 PACS number(s): 75.47.Lx, 71.30.+h, 75.10.Lp, 75.30.Et

I. INTRODUCTION

Colossal magnetoresistance (CMR) manganites are characterized by a complex interplay of charge, spin, orbital, and lattice degrees of freedom. Although manganese oxides have been known for more than 50 years,[1] their properties are still not adequately understood. After the observation of the CMR effect,[2] the modeling of complex behavior in this class of compounds has become the focus of intense research activity in modern condensed-matter theory.[3–5] These recent studies demonstrate that one has to go beyond the simple double-exchange (DE) model of Zener[6] in order to investigate a complex interplay between magnetic, orbital, charge, and lattice degrees of freedom.

Similar to perovskite manganites, monolayer $La_{1-x}Sr_{1+x}MnO_4$ and bilayer $La_{2-2x}Sr_{1+2x}Mn_2O_7$ manganites have interesting and still poorly understood physical properties. The undoped monolayer $LaSrMnO_4$ compound has the same magnetic structure as K_2NiF_4; i.e., it exhibits an *G*-type antiferromagnetic (*G*-AF) order within the layers.[7,8] This suggests a different orbital state than that realized in three-dimensional (3D) $LaMnO_3$ perovskite, where *A*-type antiferromagnetic (*A*-AF) order, with ferromagnetic (FM) *ab* planes and AF order along the *c* direction, is observed. Furthermore, unlike in $La_{1-x}Sr_xMnO_3$, in doped monolayer $La_{1-x}Sr_{1+x}MnO_4$ compounds no FM metallic phase was observed, but instead short-range magnetic correlations of various types were reported,[8–10] indicating frustrated magnetic interactions. This behavior is puzzling and has not been explained by the theory so far.

Also in bilayer $La_{2-2x}Sr_{1+2x}Mn_2O_7$ manganites a competition between magnetic interactions of different origin was observed, resulting in rather complex phase diagram,[11,12] which is a challenge for the theoretical models. At higher doping $x\sim 0.45$ the magnetic order changes from FM to *A*-AF phase. The observed phase transitions have been ascribed both experimentally[13] and theoretically[14,15] to the varying crystal-field splitting between e_g orbitals under increasing doping.

In spite of certain similarities between monolayer and bilayer compounds,[16] the magnetic correlations close to half doping ($x\sim 0.5$) are different. A metallic FM phase is observed in bilayer manganites up to $x\sim 0.45$,[17] while it is absent in monolayer compounds. While the CE-type AF order is quite pronounced at $x\simeq 0.5$ in monolayer manganites,[18] the *A*-AF phase is instead more stable in bilayer systems,[11,12] and the charge order and orbital bistripes were also observed for higher doping $0.55<x<0.6$.[19]

In the present paper, we intend to focus on the role of orbital degrees of freedom in stabilizing various types of magnetic order observed in monolayer and bilayer manganites. The behavior of e_g electrons is dominated by a large Coulomb interaction *U*. Therefore, we employ an effective spin-orbital *t-J* model similar to that derived for the 1D chain[20] and generalize it to the present situations. Thereby, we implement also Hund's exchange interaction J_H which

enforces the spin $s=1/2$ of an e_g electron to follow the t_{2g} spin $S=3/2$ at each site in the ground state. Unlike in the 1D case, the orbital e_g flavor is not conserved,[21] which enhances quantum fluctuations. They contribute to intersite correlations, and we show that a close relationship between orbital and spin correlations nevertheless persists in the ground state and at low temperature.

The previous theoretical studies revealed a competition between different types of magnetic order. Among them the most spectacular ones are phases with coexisting FM and AF bonds: (i) the *E*-type AF phase in undoped systems[22,23] and (ii) the CE phase at half doping ($x=0.5$). The former one has been experimentally observed for the very strongly Jahn-Teller (JT) distorted case only, which is at variance with its theoretical prediction for undistorted compounds. The mechanism of stability of the CE phase is also still under debate. While it has been shown that local JT distortions induce the CE-type AF order,[24,25] it remains unclear whether it could follow from electronic interactions alone. It was argued before that this complex type of magnetic and orbital order (OO) might either originate from conflicting phases[26] or could be stabilized by intersite Coulomb interactions.[24] Here we address these various mechanisms proposed before by presenting the evidence obtained by numerical simulations of finite clusters within a realistic electronic model including Coulomb interaction. We also show that this model gives a satisfactory description of magnetic correlations over the entire doping range.

The paper is organized as follows: In Sec. II we present the effective *t-J* orbital model in the regime of large *U* for e_g electrons, moving in 2D clusters simulating monolayer manganites or in $\sqrt{8}\times\sqrt{8}\times 2$ clusters standing for bilayer manganites. We also present shortly two numerical methods: the exact diagonalization with Lanczos algorithm used to solve the orbital model for fixed spin configurations at zero temperature ($T=0$) and its combination with Monte Carlo simulations of spin core (t_{2g}) configurations,[27] which leads to a coupled spin-orbital problem at $T>0$. In Sec. III the model for monolayer manganites is analyzed in different doping regimes. We report the phase diagrams obtained for undoped and half-doped systems and relate the obtained magnetic phases to orbital occupations and intersite orbital correlations. Thereby we highlight the interrelation between spin and orbital order and their dependence on increasing doping. The study of bilayer manganites in Sec. IV is limited by the size of Hilbert space for the smallest relevant $\sqrt{8}\times\sqrt{8}\times 2$ clusters, so we discuss only undoped ($x=0$), half-doped ($x=0.5$), and strongly doped ($x>0.8$) systems. Finally, in Sec. V we summarize the numerical results and present general conclusions deduced from the present study for the physical mechanisms operating in layered manganites.

II. MODEL AND NUMERICAL METHODS

A. Orbital *t-J* model

The effective orbital *t-J* model described below follows from the model of interacting e_g electrons,

$$\mathcal{H}_0 = H_t^{(0)} + H_z^{(0)} + H_{\rm int}. \tag{1}$$

The form of the kinetic energy $H_t^{(0)}$ depends on the selected basis of orthogonal orbitals, as discussed in detail by Feiner and Oleś.[21] Here we use the conventional basis which consists of

$$|z\rangle \equiv \frac{1}{\sqrt{6}}(3z^2-r^2), \quad |x\rangle \equiv \frac{1}{\sqrt{2}}(x^2-y^2) \tag{2}$$

orbitals. In a 3D (or bilayer) manganite the kinetic energy takes the form

$$H_t^{(0)} = -\frac{1}{4}t\sum_{\langle ij\rangle\|ab,\sigma}[3c_{ix\sigma}^\dagger c_{jx\sigma} + c_{iz\sigma}^\dagger c_{jz\sigma} \mp \sqrt{3}(c_{ix\sigma}^\dagger c_{jz\sigma} + c_{iz\sigma}^\dagger c_{jx\sigma})] - t\sum_{\langle ij\rangle\|c,\sigma} c_{iz\sigma}^\dagger c_{jz\sigma}, \tag{3}$$

and the last term is absent for a monolayer. The largest hopping element *t* stands for an effective $(dd\sigma)$ element between two $|z\rangle$ orbitals along the *c* axis and originates from two consecutive *d-p* transitions over oxygen orbital between the neighboring Mn ions. The same hopping element *t* couples two equivalent directional orbitals along either the *a* or *b* axis—i.e., $3x^2-r^2$ or $3y^2-r^2$ orbitals.[21]

By considering the structural data, a uniform crystal-field splitting of e_g orbitals is expected both for a monolayer[8] and for a bilayer system.[13] Therefore, we introduce the term

$$H_z^{(0)} = \frac{1}{2}E_z\sum_{i\sigma}(n_{ix\sigma} - n_{iz\sigma}), \tag{4}$$

where $n_{i\alpha\sigma}=c_{i\alpha\sigma}^\dagger c_{i\alpha\sigma}$ is the electron number operator in the $\alpha=x,z$ orbital with spin σ at site *i*. This term describes the crystal-field splitting of e_g orbitals which follows from the geometry of layered manganites and removes the orbital degeneracy. If $E_z>0$, as in undoped $LaSrMnO_4$,[8] the $|z\rangle$ orbitals are favored.

The electron interactions between e_g electrons are given by

$$H_{\rm int} = U\sum_{i,\alpha=x,z} n_{i\alpha\uparrow}n_{i\alpha\downarrow} + \left(U-\frac{5}{2}J_H\right)\sum_i n_{ix}n_{iz} + J_H\sum_i (c_{ix\uparrow}^\dagger c_{ix\downarrow}^\dagger c_{iz\downarrow}c_{iz\uparrow} + c_{iz\uparrow}^\dagger c_{iz\downarrow}^\dagger c_{ix\downarrow}c_{ix\uparrow}) - 2J_H\sum_i \vec{s}_{ix}\cdot\vec{s}_{iz} + V\sum_{\langle ij\rangle} n_i n_j. \tag{5}$$

The spin operators $\vec{s}_{i\alpha}=\{s_{i\alpha}^+, s_{i\alpha}^-, s_{i\alpha}^z\}$ are defined by fermion operators in a standard way,

$$s_{i\alpha}^+ = c_{i\alpha\uparrow}^\dagger c_{i\alpha\downarrow}, \quad s_{i\alpha}^- = c_{i\alpha\downarrow}^\dagger c_{i\alpha\uparrow}, \quad s_{i\alpha}^z = \frac{1}{2}(n_{i\alpha\uparrow} - n_{i\alpha\downarrow}). \tag{6}$$

The on-site interactions in $H_{\rm int}$ are rotationally invariant in the orbital space and are thus described with only two parameters[28] the Coulomb element *U* and a Hund's exchange element J_H. The intersite interactions $\propto V$, where each bond $\langle ij\rangle$ is included only once, do not depend on the orbital type and thus involve total electron density operators $n_i = \Sigma_{\alpha\sigma} n_{i\alpha\sigma}$.

The Hamiltonian (1) does not include yet the t_{2g} electrons which could in principle be described again by a similar multiband Hamiltonian.[29] However, in reality t_{2g} electrons

localize due to large Coulomb interaction $U \gg t$, so it suffices to consider local spins $S=3/2$ built by three t_{2g} electron spins of either a Mn^{3+} or Mn^{4+} ion. In both cases each t_{2g} orbital is singly occupied and virtual intersite hopping processes contribute to the superexchange $\propto J'$. In this parameter regime, we also find hopping processes of e_g electrons between two Mn^{3+} ions, $d_i^4 d_j^4 \rightleftharpoons d_i^5 d_j^3$, which lead to e_g^2 configurations at site i (with e_g^2 electrons either in one or at two different orbitals) and generate the e_g part of the superexchange $\propto J = 4t^2/U$. When the system is doped, direct hopping processes are also possible for Mn^{3+}-Mn^{4+} pairs, so one finds an effective t-J model, similar in spirit to the spin t-J model derived almost three decades ago from the Hubbard model.[30]

An important difference from the Hubbard model, however, arises due to Hund's exchange $-2J_H \vec{S}_i \cdot \vec{s}_i$, which favors high-spin states at each site. Hund's exchange is close[31] to the atomic value of $J_H \sim 0.9$ eV, so is sufficiently larger than the hopping, estimated for the bilayer[15] to be $t \sim 0.48$ eV, to assume that spins of e_g electrons are aligned with the $S=3/2$ core spin formed by the t_{2g} electrons. Therefore, core spin determines a local spin quantization axis at each site i, the spins of e_g electrons can be integrated out,[27] and the effective orbital t-J model takes the form

$$\mathcal{H}(S) = H_t + H_J + H_{J'} + H_z + H_V. \tag{7}$$

This Hamiltonian may be also obtained by generalizing the effective 1D model of Ref. 20 to doped layered manganites. It depends not only on the microscopic parameters introduced above, but also on the actual configuration $\mathcal{S}$ of t_{2g} spins on the lattice which determine the hopping term H_t by the double exchange mechanism.

The first term H_t in Eq. (7) stands for the hopping of e_g electrons in the limit of large on-site Coulomb interaction $U \gg t$. Its form is given below for the monolayer and bilayer systems separately. We emphasize that by performing a rigorous projection onto the $U \to \infty$ limit[21] the orbital degree of freedom of e_g electrons survives, but in agreement with the basic idea of the spin t-J model[30] and in contrast to Eq. (3), the hopping processes are now limited to the subspace without (intraorbital and interorbital) double occupancies. The double occupancies generated in virtual charge excitations by either e_g or t_{2g} electrons contribute in second order of the perturbation theory and give the superexchange interactions $\propto J$ or $\propto J'$, respectively, contained in H_J and $H_{J'}$ terms.[31]

Similar to $LaMnO_3$,[32] the superexchange in undoped $LaSrMnO_4$ and in $La_{2-2x}Sr_{1+2x}Mn_2O_7$ is given by a superposition of several terms. The e_g term H_J favors either FM or AF spin order on a bond $\langle ij \rangle$, depending on the pair of occupied e_g orbitals at neighboring sites i and j. This makes the form of the superexchange term H_J depend both on the actual geometry in layered manganites and on the used orbital basis. As the hopping term H_t, its form depends on the system and is given below.

In contrast, the superexchange interactions induced by charge excitations of t_{2g} electrons $H_{J'}$ are identical for planar and bilayer manganites. They are frequently treated as an effective AF superexchange between $S=3/2$ core spins, although they couple *de facto* two manganese ions in high-spin configurations and thus depend on the actual total number of d electrons at both ions.[34] We have verified, however, that the t_{2g} superexchange terms derived for these different configurations are of the same order of magnitude, so in a good approximation one may indeed simulate their effect by the Heisenberg Hamiltonian with an average exchange constant $J' > 0$ between $S=3/2$ core spins which favors AF spin order; this interaction is described by the term

$$H_{J'} = J' \sum_{\langle ij \rangle} (\vec{S}_i \cdot \vec{S}_j - S^2). \tag{8}$$

For convenience, we use classical core spins $\vec{S}_i$ of unit length (compensating their physical value $S=3/2$ by a proper increase of J'); i.e., we replace the scalar products of spin operators on each bond by their average values. The classically treated $\vec{S}_i$ are represented by polar angles $\{\vartheta_i, \phi_i\}$—then the spin product on a bond $\langle ij \rangle$ is given by

$$\langle \vec{S}_i \cdot \vec{S}_j \rangle = S^2 (2|u_{ij}|^2 - 1), \tag{9}$$

where the spin orientation enters via

$$\begin{aligned} u_{ij} &= \cos\left(\frac{\vartheta_i}{2}\right)\cos\left(\frac{\vartheta_j}{2}\right) + \sin\left(\frac{\vartheta_i}{2}\right)\sin\left(\frac{\vartheta_j}{2}\right) e^{i(\phi_j - \phi_i)} \\ &= \cos\left(\frac{\theta_{ij}}{2}\right) e^{i\chi_{ij}}, \end{aligned} \tag{10}$$

depending on the angle θ_{ij} between the two involved spins and on the complex phase χ_{ij}.

The remaining terms in Eq. (7), H_z and H_V, stand for the crystal-field splitting of two e_g orbitals caused by geometry and for the nearest-neighbor Coulomb interaction. The first term

$$H_z = \frac{1}{2} E_z \sum_i (\tilde{n}_{ix} - \tilde{n}_{iz}) \tag{11}$$

involves projected density operators $\tilde{n}_{ix}$ and $\tilde{n}_{ix}$ that act in the restricted Hilbert space without (interorbital and intraorbital) double occupancies. The latter term

$$H_V = V \sum_{\langle ij \rangle} \tilde{n}_i \tilde{n}_j \tag{12}$$

is the intersite Coulomb repulsion which survives as the only term from Eq. (5). It plays a role at finite doping where it can induce charge order. Here $\tilde{n}_i$ is the total e_g electron density operator at site i which acts in the restricted Hilbert space:

$$\tilde{n}_i = \tilde{n}_{ix} + \tilde{n}_{iz}. \tag{13}$$

By construction $\langle \tilde{n}_i \rangle \leqslant 1$. We include this term in half-doped manganites and investigate in Secs. III C and III D whether it helps to stabilize the CE phase with coexisting charge order.

B. Monolayer manganites

We start with the general form of the hopping term H_t which follows from Eq. (3) for planar (monolayer) manganites in the limit of $U \gg t$,

$$H_t^{2D} = -\sum_{\langle ij\rangle\|ab} t_{i\alpha,j\beta}(\tilde{c}_{i\alpha}^{\dagger}\tilde{c}_{j\beta} + \tilde{c}_{j\beta}^{\dagger}\tilde{c}_{i\alpha}), \tag{14}$$

where an operator $\tilde{c}_{i\alpha}^{\dagger}$ creates an electron in $|\alpha\rangle$ state at site i when it is unoccupied by any other (α or β) electron—i.e., implements rigorously the restriction of the Hilbert space to the subspace with no double occupancies. Furthermore, Hund's exchange between the itinerant e_g electrons to the t_{2g} core spins is large enough to justify the restriction to the subspace of e_g electrons parallel to the local t_{2g} spin; i.e., we treat spinless fermions with an orbital flavor $\alpha = x, z$ [see Eq. (2)]. Electrons with antiparallel spins and double occupancies are treated in second-order perturbation theory (see below).

In agreement with the double-exchange mechanism,[6,35] the effective hopping strength is modulated by the scalar product of the core spins at the respective sites—it is maximal for parallel spins and vanishes when spins are antiparallel. Accepting the classical treatment of intersite correlations between core spins, we use

$$t_{i\alpha,j\beta} = t_{\alpha\beta}u_{ij}, \tag{15}$$

with u_{ij} given by Eq. (10). The first factor $t_{\alpha\beta}$ is the orbital-dependent hopping strength. Its form depends on the used orbital basis and for a given pair of orbitals $\{\alpha, \beta\}$ depends on the direction of the bond $\langle ij\rangle$, as explained below.

While a representation using three directional orbitals $|\zeta\rangle$ along each cubic direction gives the simplest expression for the hopping of e_g electrons,[21] it is more convenient to consider here the fixed orthogonal orbital basis given by Eq. (2) in a 2D geometry, for which the orbital-dependent hopping strength $t_{\alpha\beta}$ in Eq. (15) is given by

$$t_{\alpha\beta}^{a} = \frac{t}{4}\begin{pmatrix} 3 & -\sqrt{3} \\ -\sqrt{3} & 1 \end{pmatrix}, \quad t_{\alpha\beta}^{b} = \frac{t}{4}\begin{pmatrix} 3 & +\sqrt{3} \\ +\sqrt{3} & 1 \end{pmatrix}, \tag{16}$$

for a bond along the a and b cubic axes, respectively. The hopping term takes then the form

$$H_t^{2D} = -\frac{1}{4}t\sum_{\langle ij\rangle\|a,b} u_{ij}[3\tilde{c}_{ix}^{\dagger}\tilde{c}_{jx} + \tilde{c}_{iz}^{\dagger}\tilde{c}_{jz} \mp \sqrt{3}(\tilde{c}_{ix}^{\dagger}\tilde{c}_{jz} + \tilde{c}_{iz}^{\dagger}\tilde{c}_{jx}) + \text{H.c.}]. \tag{17}$$

The correlated fermion operators $\tilde{c}_{iz}^{\dagger} = c_{iz}^{\dagger}(1-n_{ix})$ and $\tilde{c}_{ix}^{\dagger} = c_{ix}^{\dagger}(1-n_{iz})$ act in the restricted Hilbert space and create a $|z\rangle$ ($|x\rangle$) electron only when site i is initially empty. The hopping term (17) describes therefore spinless fermions with an orbital flavor in a restricted Hilbert space, in analogy to the original t-J model in spin space,[30] but with an anisotropic hopping term. We emphasize that the orbital flavor is not conserved along the hopping process in dimensions higher than 1 (Ref. 36). This has important consequences for the phase diagram of the orbital Hubbard model and destabilizes the OO in doped manganites.[21]

Similar as for the undoped $LaMnO_3$ (see Ref. 32), the e_g superexchange term for undoped $LaSrMnO_4$ depends on the pair of occupied e_g orbitals at sites i and j for a given bond $\langle ij\rangle$. If the spins are in the FM configuration, the superexchange interactions do not vanish but are simply reduced to purely orbital interactions which favor alternating directional ($3z^2-r^2$-like) and planar [(x^2-y^2)-like] orbitals along every cubic direction.[37] An effective orbital superexchange model presented below originates from the complete spin-orbital model[32] that included the complete multiplet structure of the excited $d*5$ and $d*4$ states[33] and focuses on the orbital dynamics in the presence of spin fluctuations which influence orbital superexchange interactions.

The superexchange due to e_g electron excitations contains spin scalar products multiplied by orbital interactions on the bonds,[32] and the full many-body problem would require treating the coupled spin and orbital dynamics. Here we study only the *orbital correlations* and their consequences for the magnetic order by replacing the scalar products of spin operators on each bond by their average values (9), as done before in the 1D model,[20] which is equivalent to decoupling spins and orbitals in a mean-field approximation. As a result, one is treating the orbital many-body problem coupled to the classical spins.

The spin operators are replaced by their expectation values following Eq. (10). In the present case of a monolayer one finds the e_g superexchange term

$$H_J^{2D} = J\sum_{\langle ij\rangle\|ab}\left\{\frac{1}{5}(2|u_{ij}|^2+3)\left(2T_i^{\zeta}T_j^{\zeta} - \frac{1}{2}\tilde{n}_i\tilde{n}_j\right) - \frac{9}{10}(1-|u_{ij}|^2)\times\tilde{n}_{i\zeta}\tilde{n}_{j\zeta} - (1-|u_{ij}|^2)[\tilde{n}_{i\zeta}(1-\tilde{n}_j) + (1-\tilde{n}_i)\tilde{n}_{j\zeta}]\right\}, \tag{18}$$

where number operator $\tilde{n}_{i\zeta}$ refers in each case to the directional orbital $|\zeta\rangle$ along a given bond $\langle ij\rangle$ and

$$T_i^{\zeta} = -\frac{1}{2}(T_i^{z} \mp \sqrt{3}T_i^{x}) \tag{19}$$

depend on the bond direction, with the sign $-$ $(+)$ in Eq. (19) corresponding to the a (b) axis. The operators are defined by orbital $T=1/2$ pseudospin operators

$$T_i^{z} = \frac{1}{2}\sigma_i^{z} = \frac{1}{2}(\tilde{n}_{ix} - \tilde{n}_{iz}), \tag{20}$$

$$T_i^{x} = \frac{1}{2}\sigma^{x} = \frac{1}{2}(\tilde{c}_{ix}^{\dagger}\tilde{c}_{iz} + \tilde{c}_{iz}^{\dagger}\tilde{c}_{ix}), \tag{21}$$

with two eigenstates of T_i^{ζ} [see Eq. (2)]. The superexchange constant $J = t^2/\varepsilon(^6A_1)$ is determined by the lowest high-spin excitation energy $\varepsilon(^6A_1)$ at the Mn^{2+} ion.[32]

C. Bilayer manganites

The hopping term for the bilayer manganites can be written again in terms of directional orbital along the bonds by extending Eq. (17). In fact, the interlayer hopping term along c axis is then diagonal in the $\{|x\rangle, |z\rangle\}$ basis,

$$t_{\alpha\beta}^{c} = t\begin{pmatrix} 0 & 0 \\ 0 & 1 \end{pmatrix}, \tag{22}$$

and one finds

$$H_t^{\mathrm{BL}} = -\frac{1}{4}t\sum_{\langle ij\rangle\|a,b} u_{ij}[3\tilde{c}_{ix}^{\dagger}\tilde{c}_{jx} + \tilde{c}_{iz}^{\dagger}\tilde{c}_{jz} \mp \sqrt{3}(\tilde{c}_{ix}^{\dagger}\tilde{c}_{jz} + \tilde{c}_{iz}^{\dagger}\tilde{c}_{jx}) + \mathrm{H.c.}] - t\sum_{\langle ij\rangle\|c} u_{ij}(\tilde{c}_{iz}^{\dagger}\tilde{c}_{jz} + \mathrm{H.c.}). \quad (23)$$

As for a single plane, the hopping H_t describes spinless fermions with an orbital flavor in a restricted Hilbert space. In each plane the orbital flavor is not conserved along the hopping process.[21]

We apply again the same approach described above to the superexchange interaction; it leads in the present case of a bilayer system to the following expression for the e_g superexchange,

$$H_J^{\mathrm{BL}} = J\sum_{\langle ij\rangle\|ab}\left\{\frac{1}{5}(2|u_{ij}|^2+3)\left(2T_i^{\zeta}T_j^{\zeta} - \frac{1}{2}\tilde{n}_i\tilde{n}_j\right) - \frac{9}{10}(1-|u_{ij}|^2)\times\tilde{n}_{i\zeta}\tilde{n}_{j\zeta} - (1-|u_{ij}|^2)[\tilde{n}_{i\zeta}(1-\tilde{n}_j) + (1-\tilde{n}_i)\tilde{n}_{j\zeta}]\right\} + J\sum_{\langle ij\rangle\|c}\left\{\frac{1}{5}(2|u_{ij}|^2+3)\left(2T_i^{z}T_j^{z} - \frac{1}{2}\tilde{n}_i\tilde{n}_j\right) - \frac{9}{10}(1-|u_{ij}|^2)\times\tilde{n}_{iz}\tilde{n}_{jz} - (1-|u_{ij}|^2)[\tilde{n}_{iz}(1-\tilde{n}_j) + (1-\tilde{n}_i)\tilde{n}_{jz}]\right\}. \quad (24)$$

Compared to Sec. II B, it is extended by the interlayer coupling terms, with the charge and orbital operators given by $\tilde{n}_{iz}$ and T_i^z along the c axis [the remaining terms for the bonds in ab planes are the same as in Eq. (18)]. For simplicity, we neglect here the difference between the intralayer and interlayer hopping elements, although for a detailed comparison with experiment it might be necessary to include different bond lengths for each cubic direction.

D. Density distribution and intersite correlations

Below we present the physical quantities which are used to characterize electron density distribution and intersite spin and orbital correlations in the ground states and at low temperature. The density distribution in both monolayer and bilayer systems at doping x is described by average electron densities in orbital α,

$$n_{\alpha} = \frac{1}{N}\sum_i \langle\tilde{n}_{i\alpha}\rangle = \frac{1}{N}\sum_i \langle\tilde{c}_{i\alpha}^{\dagger}\tilde{c}_{i\alpha}\rangle, \quad (25)$$

with N being the number of lattice sites.

Depending on the actual parameters, we encountered several different types of magnetic order, both in monolayer and in bilayer model. The FM and AF spin interactions compete with each other, so one of them is selected by a particular type of orbital correlations. The possible generic types of magnetic order, all observed in the manganites,[3–5] are shown schematically in Fig. 1. We have investigated intersite correlations at short distance $\vec{r}$ by (i) intersite spin correlations, given by the scalar product (9) of the classical core spins,

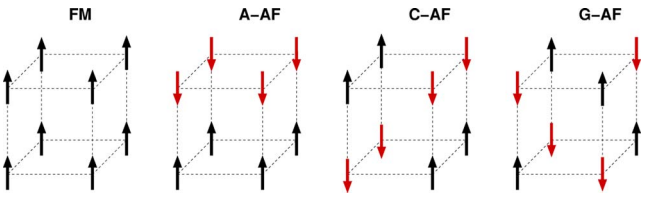

FIG. 1. (Color online) Schematic spin structures in the magnetic phases of doped manganites. The number of FM bonds decreases gradually from the FM to the G-AF phase, through the A-AF and C-AF phases, with eight and four FM bonds in a cube. For an ab monolayer, the FM and A-AF phases are equivalent.

$$\mathcal{S}(\vec{r}) = \frac{1}{N}\sum_i \langle\vec{S}_i\cdot\vec{S}_{i+\vec{r}}\rangle, \quad (26)$$

and (ii) intersite orbital correlations

$$\mathcal{T}_{\theta}(\vec{r}) = \frac{1}{N}\sum_i \langle T_i(\theta)T_{i+\vec{r}}(\theta)\rangle. \quad (27)$$

The orbital operators are defined using a particular orbital basis,

$$T_i(\theta) = T_i^z\cos\theta + T_i^x\sin\theta, \quad (28)$$

and the pseudospin operators $\{T_i^z, T_i^x\}$ at site i are given by Eqs. (20) and (21). For instance, $\theta=0$ corresponds to $T_i^zT_{i+m}^z$, $\theta=\pi/2$ to $T_i^xT_{i+m}^x$, and $\theta=2\pi/3$ to $T_i^{\zeta}T_{i+\vec{r}}^{\zeta}$, with ζ standing for the directional orbital along the a axis. The orbital correlations expected in undoped manganites are of alternating orbital (AO) type on two sublattices, which suggests that the orbital correlations $\mathcal{T}_{\theta}(\vec{r})$ defined as in Eq. (27) are predominantly negative for nearest neighbors. These correlations were investigated along the (10) and (11) directions in 2D clusters. In the bilayers we will distinguish between two different cases for both the above directions and consider either (i) both sites within the same ab layer or (ii) two sites which belong to different layers.

Spin correlations in a doped system were uniquely determined by core-spin correlations. When e_g holes are present, it is also of interest to investigate spin correlations near the hole, so we show in some cases the correlations between the two nearest-neighbor spins separated by a hole,

$$\mathcal{R} = \frac{1}{N}\sum_i \langle\vec{S}_{i-\vec{e}}(1-\tilde{n}_i)\vec{S}_{i+\vec{e}}\rangle, \quad (29)$$

where $(1-\tilde{n}_i)$ stands for the hole density at the central site i and two spins $\vec{S}_{i\pm\vec{e}}$ occupy two adjacent sites in either a or b direction.

E. Numerical methods

We employed two different but related numerical methods to investigate finite clusters described by the orbital t-J model: (i) exact diagonalization at zero temperature ($T=0$) and (ii) its combination with Markov-chain Monte Carlo (MC) simulations at finite temperature $T>0$. The ground state at $T=0$ for representative electron fillings was deter-

mined by solving the orbital *t-J* model for several possible types of spin order, using clusters with periodic boundary conditions: $\sqrt{8}\times\sqrt{8}$ and 4×4 clusters for monolayer manganites and $\sqrt{8}\times\sqrt{8}\times2$ clusters for bilayer ones. Here, the spin configurations were fixed, corresponding to different possible magnetic phases: FM, AF, *C*-AF, *E*-AF, and CE phases. To solve the orbital problem specified by the selected core-spin configuration, we employed the Lanczos algorithm, which is suitable for the very large matrices treated here and guarantees fast convergence to the ground state in each case. We then determined the global ground state by comparing the ground-state energies obtained for different magnetic phases.

At finite temperatures, we investigated the effective orbital *t-J* model by making use of a combination of Markov-chain Monte Carlo algorithm for the core spins[20] with Lanczos diagonalization. For each classical core spin configuration occurring in the MC runs, we defined the actual values of classical variables $\{u_{ij}\}$ and next employed Lanczos diagonalization to solve the many-body problem posed by the orbital model. In each case we obtained the free energy for that core-spin configuration from the few lowest eigenstates, which was next used to decide acceptance in the MC runs. We measured the Boltzmann weight of these lowest eigenstates and thereby made sure that only states with negligible weight were discarded. We emphasize that a complete many-body problem in the orbital subspace was solved, so our method differs from the standard algorithm used for noninteracting electrons which employs free-fermion formulas, as, e.g., in Ref. 38.

In the MC updates, the angle of spin rotation was optimized to keep acceptance high enough. If acceptance was very good, several rotations were performed in each update. From time to time, a complete spin flip $\mathbf{S}_i\rightarrow-\mathbf{S}_i$ was proposed. Autocorrelation analysis was employed to obtain reliable error estimates, and several hundred effectively uncorrelated samples were considered, taking particular care of burn-in and thermalization processes. Finally, wherever autocorrelations were observed to be particularly long—e.g., in symmetry-broken states like the CE phase—the method of parallel tempering[39] was employed.

III. NUMERICAL RESULTS FOR MONOLAYER MANGANITES

A. Undoped 2D clusters

In undoped manganites (at $x=0$), the hopping is entirely blocked by a large Coulomb interaction U and the nearest-neighbor Coulomb interaction V (12) is irrelevant as the electron density is $n=1$ at each site. Therefore, the Hamiltonian for a monolayer, Eq. (7), reduces to the superexchange terms given by Eqs. (8) and (18), accompanied by the crystal-field splitting of e_g orbitals, given by Eq. (11). Therefore, the ground state for finite J is determined by only two parameters J'/J and E_z/J. The phase diagram of the spin-orbital model (7) in the (J',E_z) plane obtained by exact diagonalization of a 4×4 cluster at $T=0$ is shown in Fig. 2.

A particularly simple result is obtained at $J'=E_z=0$, where the FM phase has the lowest energy. As $u_{ij}\equiv1$ in a ferromagnet, only the first term in the e_g superexchange (18) survives and stabilizes the AO order. Of course, this phase is also stable in an unphysical regime[40] of negative $J'<0$ in a broad range of crystal-field splitting (see Fig. 2). This coexistence of AO order with the FM spin correlations is generic—it confirms the trend observed before in the 1D model[20] and on ladders,[41] and agrees with the Goodenough-Kanamori rules.[42] When a robust AO state develops at the orbital degeneracy ($E_z=0$), the FM phase extends to a broader range of $J'\gtrsim0$ than at $|E_z|>0$.

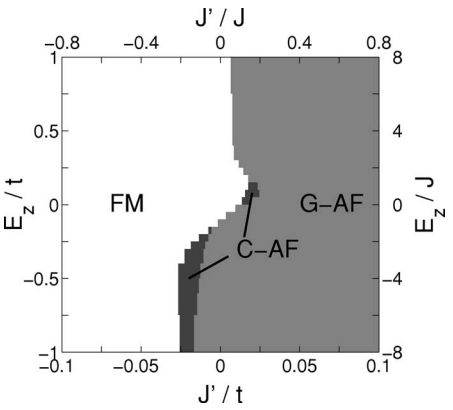

FIG. 2. Phase diagram for the undoped layered manganites ($x=0$), with the stability regions of FM, *G*-AF, and *C*-AF phases (see Fig. 1) in the (J',E_z) plane, as obtained at $T=0$ with a 4×4 cluster. The core-spin superexchange J' and the crystal-field splitting E_z are given both in units of J and in units of t for $J=0.125t$.

As the FM and AF terms in the e_g superexchange (18) compete with each other, the *G*-AF phase has only slightly higher energy than the FM one at $E_z=0$, so it can be rather easily stabilized by finite AF t_{2g} superexchange $J'>0$. One finds indeed a transition to AF order at $J'\gtrsim0.0091t$ (we use below $t=1$ as an overall energy unit). Note, however, that near orbital degeneracy ($E_z\sim0$) a robust AO state develops as both orbitals can participate in an equal amount, and therefore the FM phase extends here to higher values of J' than at large orbital splitting $|E_z|$. Therefore, the crystal-field energy may easily tip the energy balance and stabilize a different type of magnetic order, although E_z controls primarily the charge distribution. Indeed, at large $|E_z|$ only one of e_g orbitals is selected and AO order is hindered, so the AF phase is favored and occurs already for smaller J' than at $E_z=0$ (see Fig. 2). For $E_z<0$, $|x\rangle$ orbitals are occupied and one finds large AF e_g superexchange—therefore in this case the AF phase is favored even for $J'=0$. In contrast, when $|z\rangle$ orbitals are favored for $E_z>0$, the e_g superexchange is weaker by a factor of $(t_{xx}/t_{zz})^2=9$ and the *G*-AF phase can be stabilized only by $J'\simeq0.01t$. Moreover, one finds that the competition between the FM and AF orders may induce the *C*-AF phase in the crossover regime between the FM and AF phases. We note that the *C*-AF phase is expected to be further stabilized by finite cooperative JT distortions.

In order to get more insight into the phases of Fig. 2, we investigated orbital correlations between first and second neighbors. Let us first look at the ferromagnetic phase at $E_z=0$: Since there is no hopping at $x=0$ and since all bond are FM (i.e., $u_{ij}\equiv1$), the Hamiltonian comprises only the

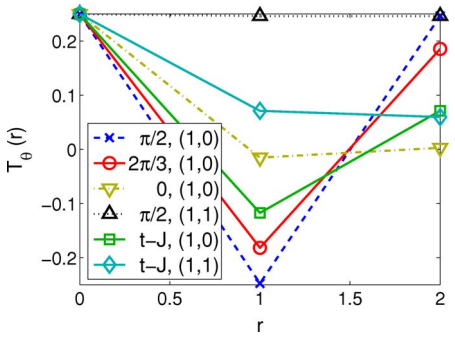

FIG. 3. (Color online) Orbital correlations $\mathcal{T}_\theta(\vec{r})$, Eq. (27), in the (01) direction in the FM phase, as obtained for the undoped 4×4 cluster using T_i^ζ operators defined for different bases of orthogonal orbitals: $\theta=0$—$\{|x\rangle,|z\rangle\}$; $\theta=\pi/2$—$\{(|x\rangle\pm|z\rangle)/\sqrt{2}\}$, $\theta=2\pi/3$—$\{|\zeta\rangle,|\xi\rangle\}$. The latter choice involves directional orbitals within the ab plane. Orbital correlations shown in the (11) direction for $\theta=\pi/2$ demonstrate an almost perfect AO order. Parameters: $E_z=J'=0$. Spin correlations obtained for the spin model (i.e., the Heisenberg model for $s=1/2$) on a 4×4 cluster at $n=1$ are shown for comparison by squares and diamonds.

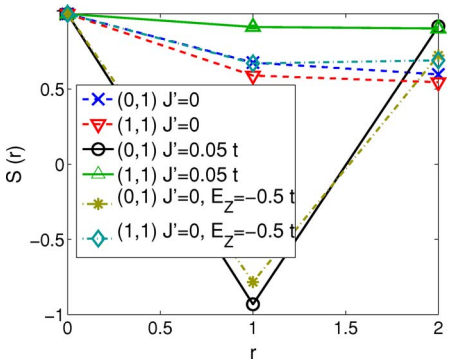

FIG. 4. (Color online) Spin correlations $\mathcal{S}(\vec{r})$, Eq. (26), in the undoped monolayer, as obtained in MC simulations with a 4×4 cluster for $J'=0$ and $E_z=0$ (FM correlations) and for $J'=0$, $E_z=-0.5t$, as well as for $J'=0.05t$, $E_z=0$ (both sets give AF correlations). Error bars are smaller than symbol sizes. Parameters: $J=0.125t$, $\beta t=100$.

first term of Eq. (18). While it looks similar to a spin t-J model (or in this undoped case the Heisenberg model for $s=1/2$), the important difference is that the orbital model is not isotropic. As a consequence, the orbital correlations (27) differ markedly from those familiar from the isotropic spin t-J model and depend on the considered orbitals basis. They are shown in Fig. 3 for various orbitals parametrized by the angle θ [see Eq. (28)], and one finds that almost no correlations are found when angle $\theta=0$ is selected—i.e., for $\mathcal{T}_{ij}(0)=\langle T_i^z T_j^z\rangle$. In contrast, orbital correlations designed to detect the AO order, with angle $\theta\sim\pi/2$, are quite distinct, such as, for instance, for $\theta=2\pi/3$, when correlations between two directional $3x^2-r^2/3y^2-r^2$ orbitals within the plane are measured by $\mathcal{T}_{ij}(2\pi/3)=T_i^\zeta T_j^\zeta$. As this correlation function is negative, one finds the OO close to staggered directional orbitals on two sublattices, with $\theta_{i\in A}=\theta$ and $\theta_{j\in B}=-\theta$—i.e.,

$$|\theta\rangle_{i\in A}=\cos\left(\frac{\theta}{2}\right)|z\rangle_i+\sin\left(\frac{\theta}{2}\right)|x\rangle_i, \tag{30}$$

$$|\theta\rangle_{j\in B}=\cos\left(\frac{\theta}{2}\right)|z\rangle_j-\sin\left(\frac{\theta}{2}\right)|x\rangle_j. \tag{31}$$

Remarkably, the orbital correlations defined by the directional orbitals on two sublattices (−0.1816) are very similar to those obtained with $\mathcal{T}_{ij}(2\pi/3)$ (−0.1892), but both types of OO do not minimize the negative orbital superexchange. A common large negative contribution to the above values comes from the $\langle T_i^x T_j^x\rangle=-0.1854$ correlation—it decreases further when the angle θ is varied towards $\theta=\pi/2$, where the orbital correlations reach a minimal value, $\mathcal{T}_{ij}(\pi/2)=\langle T_i^x T_j^x\rangle=-0.2472$. Thus, in agreement with earlier findings,[37,41] the quantum correction to the classical value −0.25 is very small indeed due to the gap which opens in orbital excitations in the present 2D case. This means that robust AO order with orbitals of the form $(|x\rangle\pm|z\rangle)/\sqrt{2}$ is realized in an undoped monolayer without crystal-field splitting, similar to the OO in the 3D model,[32] if this monolayer has FM spin order.

For comparison, we also included in Fig. 3 the spin correlation (26) of the spin t-J model—it is isotropic due to SU(2) symmetry, and quantum fluctuations keep the value of $\mathcal{S}(1)$ for the (10) direction well above the classical value −1/4. In contrast, for the orbital model the optimal correlations found for $\theta=\pi/2$ almost attain the classical value and thus show almost perfect OO. An additional advantage of this robust OO for the present calculations is that the ground-state energy E_0 hardly depends on the cluster size—one finds for the FM phase ($u_{ij}=1$) at $E_z=0$: $E_0=-0.21970t$ for $\sqrt{8}\times\sqrt{8}$, $-0.21968t$ for $\sqrt{10}\times\sqrt{10}$, and $-0.21967t$ for 4×4 cluster; i.e., finite-size effects are negligible. When the AF order is considered instead ($u_{ij}=0$), the second term in the orbital superexchange, Eq. (18), dominates and thus almost only in-plane $|x\rangle$ orbitals are occupied. Finite-size effects are here again small, with $E_0=-0.183\,35t$ for $\sqrt{8}\times\sqrt{8}$, $-0.183\,34t$ for $\sqrt{10}\times\sqrt{10}$, and $-0.183\,33t$ for 4×4 cluster.

In the present model one does not find the E-AF phase, which has been experimentally observed for strongly JT-distorted $HoMnO_3$.[43] We attribute this to the fact that the present model does not include phonons and thus rather describes manganites with little or no JT distortion. The E-AF phase was found before in MC simulations using a model neglecting on-site Coulomb repulsion in the regime of large J' and small electron-phonon coupling λ, where it was stabilized by the kinetic energy.[23,44] It could argued, however, that this is not a realistic description, as local Coulomb repulsion (intraorbital U and interorbital U') inhibits e_g electron motion for the $x=0$ ($n=1$) limit, so the microscopic mechanism of the E-AF phase in $HoMnO_3$ remains puzzling.

While ground-state calculations comparing different ordered phases lead to valuable insights at relatively low computational cost, one has to realize that such calculations at $T=0$ are still necessarily limited by the authors' imagination concerning the magnetic phases to consider. We therefore complemented them by unbiased MC simulations for a few parameter sets at low temperature $\beta t=100$. Figure 4 shows the spin correlations (for core t_{2g} spins) obtained from the

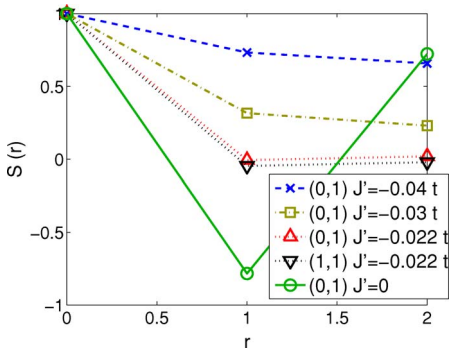

FIG. 5. (Color online) Spin correlations $\mathcal{S}(\vec{r})$, Eq. (26), in the undoped monolayer as in Fig. 4, but for decreasing J' from $J'=0$ (AF correlations) to $J'=-0.04t$ (FM correlations). Parameters: $J=0.125t$, $E_z=-0.5t$, $\beta t=100$.

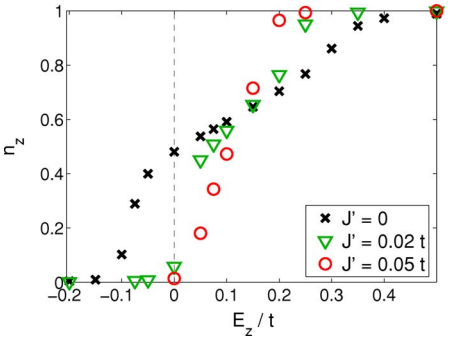

FIG. 6. (Color online) Electron density in the $|z\rangle$ orbital perpendicular to an *ab* plane of a monolayer manganite for increasing crystal-field splitting E_z [see Eq. (11)], as obtained from MC simulations of undoped ($n=1$) $\sqrt{8}\times\sqrt{8}$ clusters with various values of J'. Parameters: $J=0.125t$, $\beta t=100$.

MC data for one ($E_z=J'=0$) example of the FM and two ($E_z=0$, $J'=0.05t$ and $E_z=-0.5t$, $J'=0$) of the AF phase. These data are complemented by the orbital correlations (not shown) which correspond closely to the ground-state results. Both spin and orbital correlations weaken with rising temperature, as discussed elsewhere,[45] but for realistic values of $J'\simeq 0.02t$ spin correlations melt somewhat faster even in the present case when the orbital interactions induced by the JT effect are neglected.

The situation is somewhat different for the *C*-AF phase obtained by exact diagonalization at $T=0$ for $E_z\lesssim -0.2t$ (see Fig. 2). We analyzed the spin correlations $\mathcal{S}_{ij}$ at low temperature for $E_z=-0.5t$ and a few selected values of $J'=0$, $-0.022t$, $-0.03t$, $-0.04t$ (Fig. 5). For $J'=0$ one finds AF correlations and for $J'=-0.04t$ FM ones, both in accordance with the ground-state phase diagram of Fig. 2. However, the phase transition between these phases (the value $J'=-0.022t$ lies right in the middle of the *C*-AF region) does not occur via the *C*-AF phase at finite temperature, which would give an AF signal for $\vec{r}=(1,1)$. Neither do the intermediate values of J' exhibit the *E*-AF phase, which should show an AF signal for $\vec{r}=(0,2)$ and has only slightly higher energy than the *C*-AF phase at $T=0$, nor do the MC snapshots for this parameter range and $\beta t=100$ suggest any other ordered phase. However, the temperature $\beta t=100$ might be still too high to allow for longer-range magnetic correlations precisely in the crossover regime. In conclusion, we have established that the AF and FM phases of Fig. 2 are well supported by the MC results, while we believe the transition between them might occur either via the *C*-AF phase or with phase separation.[22]

In order to understand better the phase diagram of Fig. 2 it is instructive to consider the orbital occupation. When a positive crystal field ($E_z>0$) is applied, $|z\rangle$ orbitals which stick out of the *ab* plane are favored (see Fig. 6). For the AF phase at $J'=0.05t$, a relatively small value $E_z=0.15t$ suffices already to switch the density distribution from mainly $|x\rangle$ (at $E_z=0$) to mainly $|z\rangle$ orbital occupation. The width of the crossover regime from $|x\rangle$ to $|z\rangle$ orbital occupation increases with decreasing J'. As discussed above, the FM phase is characterized by an approximately equal occupation of both orbitals at $E_z=0$. When both e_g orbitals mix, the AO order found in the FM phase at $J'=0$ is robust and a rather large value of crystal field $E_z\simeq 0.4t$ is needed to enforce complete $|z\rangle$ polarization. This large value of E_z reflects the cooperative character of the FM spin and AO order. At the same time, a negative crystal field $E_z\lesssim -0.1t$ is needed in order to enforce complete $|x\rangle$ polarization, while this transition occurs at $E_z\simeq 0$ for $J'=0.02t$.

Note that in the ferro orbital (FO) phase with $|x\rangle$ orbitals occupied (at $E_z<-0.2t$, the AF spin order is induced even for $J'=0$; see the spin correlations in Fig. 4 and the phase diagram of Fig. 2). This provides another example of complementary spin and orbital correlations that agree with Goodenough-Kanamori rules.[42] At $J'=0.02t$ one finds an intermediate situation in this respect—while both at $E_z\leqslant 0$ and $E_z\geqslant 0.25t$ the magnetic order is AF and dictated by J', with either $|x\rangle$ or $|z\rangle$ orbitals being filled, in the transition region at $0<E_z<0.25t$ one finds AO $(|x\rangle\pm|z\rangle)/\sqrt{2}$ order, but rather unclear magnetic structure at $\beta t=100$. This shows again that magnetic correlations are typically lost at lower temperature, particularly when different conflicting trends in magnetic interactions compete with each other.

Experimentally, the AF order with e_g electrons occupying mainly $|z\rangle$ orbitals was found[8] in a monolayer-undoped compound $LaSrMnO_4$, which we interpret as a consequence of sufficiently large positive crystal field, $E_z\sim 0.5t$, induced by the 2D structure. With growing temperature $|x\rangle$ occupation rises,[8] as we also observed in the MC simulations.[45]

B. Stability of the CE phase at half doping

Next we investigate the spin correlations at half doping ($x=0.5$) and determine the range of stability of the CE phase, which was observed in a monolayer $La_{0.5}Sr_{1.5}MnO_4$ compound.[9,10] We have performed ground-state ($T=0$) calculations using the three clusters shown in Fig. 7, with periodic boundary conditions. Because of the large Hilbert space at half-filling, MC simulations could be completed only for $\sqrt{8}\times\sqrt{8}$ clusters [for the cluster geometry and one possible realization of the CE phase; see Fig. 7(a)]. In these simulations, we obtained the CE phase for some parameters—e.g.,

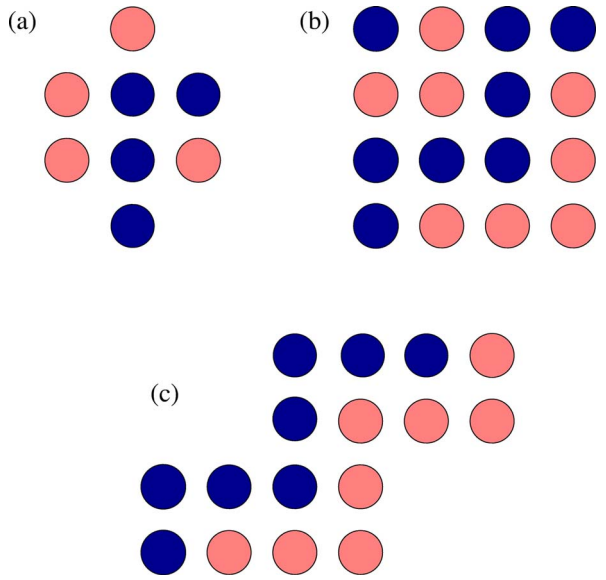

FIG. 7. (Color online) Clusters used to investigate the CE phase at half doping ($x=0.5$): (a) $\sqrt{8}\times\sqrt{8}$, (b) 4×4, and (c) 2×8. Dark (light) shading indicates possible realizations of staggered FM zigzag chains in the CE phase.

for $J=0.125t$, $E_z=0$, either for $J'=0.05t$ and $V=0$ or for $J'=0.025t$ and $V=t$. A typical MC snapshot is shown in Fig. 8. As we have used periodic boundary conditions, one recognized the CE phase in an $\sqrt{8}\times\sqrt{8}$ cluster repeated several times.

The spin correlations resulting from the MC runs are compared to those of the ideal CE phase (exact diagonalization at $T=0$) in Fig. 9, and one finds an almost perfect agreement—in both cases, AF and FM signals cancel along the (01) direction, because of the different possible realizations of the CE phase, but along the diagonal (11) direction the spin correlation reaches −0.5. (For the Monte Carlo simulations in these parameter regimes, we used parallel tempering[39] in order to sample the different symmetry-related realizations correctly.)

On the one hand, the occurrence of the CE phase for classical spins even *without* the cooperative JT effect in the present study is in contrast to the results obtained recently for quantum-mechanical $S=1/2$ core spins,[46] where quantum fluctuations suppress the CE phase. While it is not completely clear whether $S=3/2$ core spins are better approximated by more quantum $S=1/2$ or by classical $S\to\infty$ spins, the latter has been shown to be an excellent approximation in the one-orbital model in one dimension.[47] On the other hand, a similar model, but including phonons and *without* on-site Coulomb repulsion between the e_g electrons, was treated on a 4×4 site cluster [see Fig. 7(b)] in Ref. 56. Because the on-site Coulomb repulsion was not included, unrealistically large $J'>0.2t$ or rather strong electron-phonon coupling $\lambda \gtrsim 1.75$ was necessary to stabilize the CE phase. Although this result could still be improved by considering larger clusters, it highlights already the importance of strong Coulomb interactions for obtaining physically relevant results.

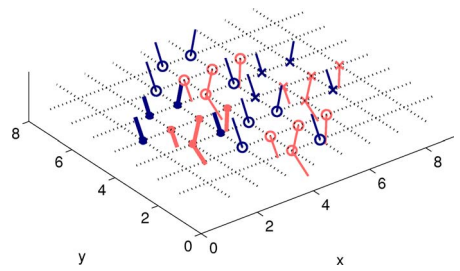

FIG. 8. (Color online) MC snapshot obtained for doping $x=0.5$, with spin directions indicated by lines. Four $\sqrt{8}\times\sqrt{8}$ clusters are shown (heavy lines indicate the original cluster), and one clearly recognizes the magnetic order in the CE phase. Parameters: $J=0.125t$, $J'=0.05t$, $E_z=V=0$, $\beta t=100$.

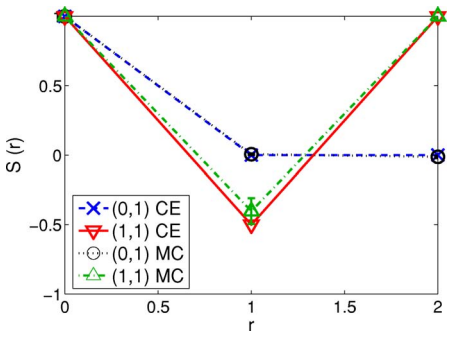

FIG. 9. (Color online) Spin-spin correlation $\mathcal{S}(\vec{r})$, Eq. (26), for the ideal CE phase and the MC data for an $\sqrt{8}\times\sqrt{8}$ cluster. There is one AF signal at (1,1). Parameters: $J=0.125t$, $J'=0.05t$, $E_z=V=0$, $\beta t=100$.

When FM and AF interactions occur simultaneously at different bonds in *ab* planes, one has to investigate the stability of the CE phase by comparing it with the *C*-AF phase which has the same amount of FM and AF bonds. We have found that at $J=0.125t$ the *C*-AF phase has higher energy than the CE one for small clusters of eight sites and the same holds true for larger 4×4 clusters. However, it has been pointed out that finite-size effects are important,[48] so one would like to investigate still larger clusters, at least at $T=0$.

As a first step, we exploit the quasi-1D nature of the two phases and investigate 8×2 clusters instead of 4×4 ones (at present, we cannot treat more than 16 sites): (i) a ladder for the *C*-AF phase and (ii) the cluster shown in Fig. 7(c) for the CE phase. While the energy of the CE phase hardly changes with cluster topology, the one of the *C*-AF phase is considerably lowered, albeit still higher than that of CE phase (see Table I). To make the ground-state calculations more conclusive and to eliminate systematic errors, it is therefore indeed necessary to investigate finite-size effects.

Due to the magnetic order in both *C*-AF and CE phases, hopping occurs only along a 1D path, so chains can be investigated instead of 2D lattices. In this way larger systems could be reached. Taking the kinetic energy for a FM chain,

$$H_t^{\mathrm{C/CE}} = -\frac{1}{4}t\sum_i [3\tilde{c}_{i,x}^\dagger \tilde{c}_{i+1,x} + \tilde{c}_{i,z}^\dagger \tilde{c}_{i+1,z} \pm \sqrt{3}(\tilde{c}_{i,x}^\dagger \tilde{c}_{i+1,z} + \tilde{c}_{i,z}^\dagger \tilde{c}_{i+1,x}) + \mathrm{H.c.}], \quad (32)$$

we considered two different geometries: (i) the *C*-AF phase

TABLE I. Ground-state energies as obtained for the *C*-AF and CE phases with different clusters of Fig. 7 and for 1D chains simulating these phases, for three representative values of E_z. In case of 2×8 clusters, a ladder was used for the *C*-AF phase and the cluster shown in Fig. 7(c) for the CE phase. Parameters: $J=0.125t$, $V=0$.

E_z/t	Phase	$\sqrt{8}\times\sqrt{8}$	4×4	2×8	4×1	8×1
0.0	CE	−0.6452	−0.6624	−0.6624	−0.6466	−0.6641
	C-AF	−0.5366	−0.5366	−0.6330	−0.5366	−0.6365
0.5	CE	−0.7371	−0.7358	−0.7358	−0.7372	−0.7357
	C-AF	−0.6220	−0.6221	−0.7068	−0.6140	−0.7076
−0.5	CE	−0.5895	−0.6238	−0.6238	−0.5917	−0.6269
	C-AF	−0.5183	−0.5184	−0.6045	−0.5159	−0.6077

with a chain along *b* axis—i.e., taking + sign for the interorbital hopping in Eq. (32)—and (ii) a zigzag path chosen instead for the CE phase, which leads to a sequence $(b,b,a,a,b,b,\ldots)$ of bond directions and therefore to the phase sequence $(+,+,-,-,+,+,\ldots)$ in the hopping.

Because the FM order within the chains (in either CE or *C*-AF phase) is perfect at zero temperature ($u_{ij}=1$), the superexchange along them contains only one term,

$$H_J^{\mathrm{FM}} = J\sum_i \left(2T_i^{\zeta}T_{i+1}^{\zeta} - \frac{1}{2}\tilde{n}_i\tilde{n}_{i+1}\right), \tag{33}$$

where ζ is the directional orbital along the bond direction—i.e., along *b* in the *C*-AF phase and alternating between *a* and *b* in the CE phase. However, superexchange via AF bonds also contributes and these *interchain coupling* terms could be crucial for stabilizing one or the other phase.[49] We therefore embedded the chains and included into the effective 1D Hamiltonian additional AF superexchange terms,

$$H_J^{\mathrm{AF}} = \frac{3}{5}J\sum_i \left(2T_i^{\bar{\zeta}}T_{i+1}^{\bar{\zeta}} - \frac{1}{2}\tilde{n}_i\tilde{n}_{i+1}\right) - J\sum_i [\tilde{n}_{i\bar{\zeta}}(1-\tilde{n}_{i+1}) + (1-\tilde{n}_i)\tilde{n}_{i+1\bar{\zeta}}] - \frac{9}{10}J\sum_i \tilde{n}_{i\bar{\zeta}}\tilde{n}_{i+1\bar{\zeta}}, \tag{34}$$

where $\bar{\zeta}$ is the directional orbital *perpendicular* to the chosen path—i.e., couples nearest-neighbor sites on two adjacent chains. The form of Eq. (34) is motivated by the fact that a bridge site on one chain (in the CE phase) lies always next to two corner sites of the neighboring chains in the *ab* plane. By symmetry, these should be equivalent to the corner sites on the considered chain, which are again the nearest-neighbor sites to a given bridge site. The energy of the *C*-AF phase is evaluated with a similar term.

In order to check the validity of this one-dimensional approach, we compare the energies obtained on small 2D clusters (third to fifth columns in Table I) to those obtained on short chains of four and eight sites (last two columns in Table I). For the CE phase, $L=4$ corresponds to the chain length encountered in a $\sqrt{8}\times\sqrt{8}$ cluster and the energies differ indeed only by $\sim 0.0015t$. For the *C*-AF phase, $L=4$ corresponds to either $\sqrt{8}\times\sqrt{8}$ or 4×4 cluster and one also finds

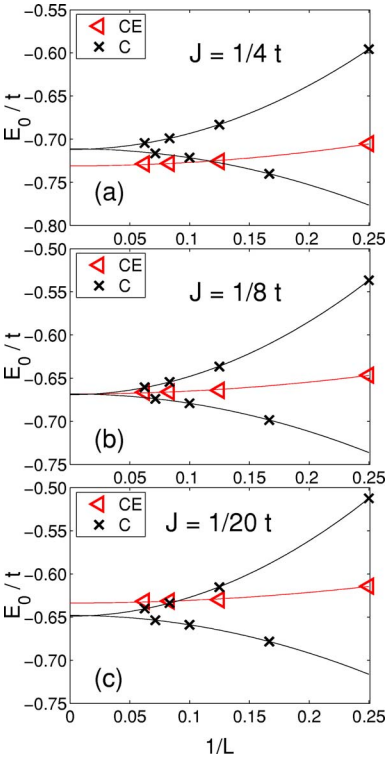

FIG. 10. (Color online) Finite-size extrapolation of the ground-state energy E_0 for the *C*-AF and CE phases on chains of different length $L\leqslant 16$, as obtained at $T=0$ for different values of J: (a) $J=0.25t$, (b) $J=0.125t$, and (c) $J=0.05t$. The data for the *C*-AF phase alternate between the chains of length $L=4n$ and $L=4n+2$, with n integer. Parameters: $J'=E_z=V=0$.

remarkably good agreement. The difference is larger for $L=8$ and the ladderlike clusters, but it seems still reasonable to investigate systematically the Hamiltonian comprising the three terms given in Eqs. (32)–(34) on chains of different length.

The results for chains of various lengths were next extrapolated to the $1/L\to 0$ limit (see Fig. 10). An excellent fit was obtained using a quadratic dependence of the ground-state energy on the inverse chain length, $E_0=E_{0,\infty}+k\times\frac{1}{L^2}$. In this way we deduced the extrapolated energy values $E_{0,\infty}$. As only directional orbitals oriented along the chain contribute to the kinetic energy in the *C*-AF phase, this energy is not influenced by *U*. Consequently, one finds that large on-site repulsion *U*—i.e., small *J*—favors the *C*-AF phase (see also Refs. 48 and 49). Furthermore, it appears that the energies of both phases are so close to each other for $J\sim t/8$ that one cannot distinguish between these phases and decide on the nature of magnetic correlations in the ground state. This result is not strongly affected by a uniform crystal field E_z either—the energies of the two magnetic phases are again very similar for $J=t/8$.

As the commonly used picture of the CE phase assumes charge order, one expects that it to be stabilized by nearest-neighbor Coulomb repulsion *V*. The extrapolation to $1/L\to 0$ gives indeed lower energies of the CE phase for $V>0$, but the effect of *V* remains *surprisingly small*. The reason is that the second of the AF terms in Eq. (34) already induces

some charge order in the C-AF phase as well, and therefore its energy does not suffer much from Coulomb repulsion V. If, on the other hand, V becomes too large, it hinders electron motion along the FM chains in both the C-AF and CE phases and thus affects both of them, even favoring the C-type AF phase for very large $V \gtrsim 1.5t$.

C. Orbital and charge order at half doping

When the magnetic order of CE type occurs, the sites along each FM zigzag chain are nonequivalent, and one expects that holes are predominantly found at the corner sites.[22–24] However, in the present finite cluster calculations different CE patterns mix with each other and the holes cannot be detected using just density operators. This information can be extracted only from intersite correlations, such as, for instance, the spin-hole-spin correlation $\mathcal{R}$ which measures the spin-spin correlations across a central site occupied by the hole [see Eq. (29)]. For the clusters shown in Fig. 7 we consider the FM zigzag chains along the (11) direction. On the one hand, the sites to the "right" and "left" of a corner site along the a axis—i.e., (10) direction—have opposite spin, as well as those "above" and "below" it along the b axis—i.e., (01) direction. For the bridge sites, on the other hand, the neighboring spins along either direction have the same sign. In the CE phase, negative values of $\mathcal{R}$ indicate therefore that holes occupy corner rather than bridge sites.[50]

We have calculated the correlation function $\mathcal{R}$ for the ground state; i.e., first the spins were set into the zigzag CE pattern and next the resulting orbital Hamiltonian was solved with Lanczos diagonalization. In the absence of nearest-neighbor Coulomb repulsion (at $V=0$), we then found $\mathcal{R}=-0.087$, from which we deduced the electron density at corner sites $n_c \simeq 0.413$ vs $n_b \simeq 0.587$ on the bridge sites. (The MC data at low temperature $\beta t=100$ with $J'=0.05t$ and $E_z=V=0$ give a somewhat weaker spin and charge order with $\mathcal{R}=-0.0757\pm0.001$.) The electrons at the bridge sites are almost exclusively in the directional $3x^2-r^2$ ($3y^2-r^2$) orbitals along the a (b) axis—i.e., along the direction of the zigzag chain. In contrast, the electrons at corner sites are more evenly distributed over both orbitals in the CE ground state (at $E_z=0$), with $n_x^c=0.2307$ in $|x\rangle$ vs $n_z^c=0.1823$ in $|z\rangle$ orbital, respectively.

These findings—i.e., the relatively small difference in the density at bridge and corner sites and the occupation of the directional orbitals—are in contrast to some experimental results.[51,52] However, the OO similar to our findings was also reported,[16,53,54] and one expects that rather extreme charge modulation, with holes at corner sites and e_g electrons in bridge positions, should be excluded as then the FM double exchange which stabilizes the CE phase would be lost. Therefore, the charge order with alternating Mn^{3+} and Mn^{4+} ions has been challenged and an intermediate valence picture with only small density variations has been suggested both in experimental[55] and in theoretical studies.[24,56–58]

In this section we would like to address as well the recent controversy concerning the type of the OO in the CE phase. We analyzed the orbital occupation in the $3x^2-r^2$ and $3y^2-r^2$ orbitals for various values of the crystal-field splitting

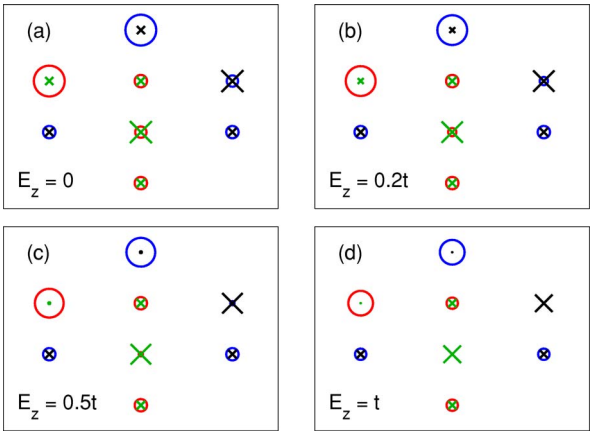

FIG. 11. (Color online) Orbital structure for the CE phase at $T=0$, with circles (crosses) for $3x^2-r^2$ ($3y^2-r^2$) orbitals, as obtained for (a) $E_z=0$, (b) $E_z=0.2t$, (c) $E_z=0.5t$, and (d) $E_z=t$. The size of circles and crosses is proportional to the electron density in a given orbital. Parameters: $J=0.125t$, $V=0$.

$E_z \geqslant 0$ (Fig. 11). At $E_z=0$ the electrons at the bridge sites are found in the orbitals parallel to the FM chain [Fig. 11(a)]—i.e., in $3x^2-r^2$ or $3y^2-r^2$—as discussed above. One finds that the corresponding orthogonal orbital is practically empty—e.g., y^2-z^2 orbitals at the bridge sites with both neighboring FM bonds along the x direction. However, a large density is found within these orbitals at the remaining bridge positions (in y^2-z^2 orbitals on those sites where the FM chains have the bonds along the y direction), which is due to the considerable overlap between the $3y^2-r^2$ and y^2-z^2 orbitals. Thus, the $3x^2-r^2/3y^2-r^2$ order appears to be qualitatively similar to the z^2-x^2/y^2-z^2 order. In the present case, however, we would rather identify it as $3x^2-r^2/3y^2-r^2$ order because the occupation on the bridge sites is almost exclusively in the directional orbitals.

When the crystal field E_z increases, the orbital occupation changes (see Fig. 11). Not surprisingly, the density in the $3z^2-r^2$ orbitals (not shown) has increased, which modifies the type of the OO—one finds now that the *directional* orbital is the one which is empty on some sites, which means that the electron on a bridge site has moved from the $3x^2-r^2$ ($3y^2-r^2$) into the z^2-x^2 (y^2-z^2) orbital. This situation could therefore be considered as representing (z^2-x^2/y^2-z^2)-type order. The observed transition from the former (at $E_z=0$) to the latter (at $E_z=1$) phase is driven by the crystal field and is gradual (see Fig. 11). Therefore, it may be argued that the combination of spin and orbital structure in Fig. 1 of Ref. 52, given schematically in Fig. 12(a), is incorrect: In this picture, the FM spin chains run perpendicular to the occupied z^2-x^2 (y^2-z^2) orbitals at the bridge sites—i.e., in the y (x) direction. Instead, our data indicate that the FM chains run as shown in Fig. 12(b)—i.e., in the x direction, where the z^2-x^2 orbital is occupied for large $E_z>0$ and along the y direction for the y^2-z^2 sites.

Another difference between the analysis performed in Ref. 52 and our results is that charge order is not perfect in our case, as it was assumed in their analysis. This does not influence the OO, however—for $V=t$ the charge order is enhanced (i.e., the electron density at bridge sites increases)

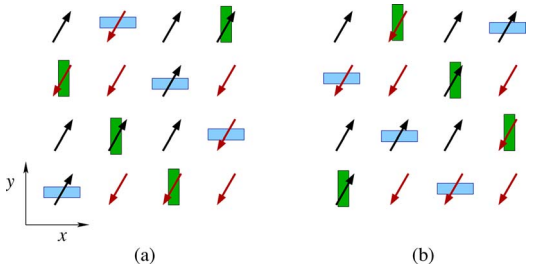

FIG. 12. (Color online) Possible orbital and spin structure for the CE phase, as suggested (a) in Fig. 1 of Ref. 52 and (b) from our calculations. The orientation of the rectangles indicates the type of occupied orbital—horizontal z^2-x^2 or vertical y^2-z^2.

without greatly affecting the type of the OO (not shown). Here we would like to emphasize that our findings concerning the nature of spin and OO, as well as rather weak charge order, agree with recent Hartree-Fock calculations on the multiband *d-p* model,[58] indicating that the local Coulomb interactions and superexchange suffice already to stabilize the CE phase. There is no doubt, however, that oxygen distortions also contribute to the stability of this phase[46,58] and would expand the regions of the CE phase in the phase diagrams shown in the next section. At the same time realistic oxygen distortions would also modify somewhat the type of occupied orbitals, but the essential features of the orbital order in the CE phase [see Fig. 12(b)] would remain the same.

The facts that (z^2-x^2/y^2-z^2)- and $(3x^2-r^2/3y^2-r^2)$-type orbital orders are qualitatively similar[59] and that one can come from one to the other one by adding a constant crystal field are consistent with the results reported in Ref. 51, where a shear-type distortion (alternating *contractions* along the x/y axes) has been found more plausible than a JT-type OO (alternating *elongations* along the x/y axes). In the shear-type order, the out-of-plane Mn-O bond is of a similar length as the *longer* in-plane bond, while it is comparable to the *shorter* bond in the JT-like case. Variation of the out-of-plane bond, equivalent to $E_z>0$ in our model, can therefore lead from one scenario to the other. In closing, we remark that the kinetic energy favors $3x^2-r^2/3y^2-r^2$ occupation as this maximizes the hopping. On-site Coulomb repulsion inhibits the kinetic energy, and when we weaken Coulomb repulsion from $U=8t$ $(J=0.125t)$ to $U=4t$ $(J=0.25t)$ and thus enhance the kinetic energy, we indeed find that a stronger E_z is needed to induce (z^2-x^2/y^2-z^2)-type OO. This is in accordance with the usual experience based on comparing local density approximation (LDA) with LDA+U calculations,[51] where inclusion of on-site interaction has likewise been found to be crucial in stabilizing shear type over the JT type of OO.

D. Phase diagrams at half doping

Our results on the stability of magnetic phase at $x=0.5$ were collected in the phase diagrams of Fig. 13 for two representative values of the on-site Coulomb repulsion, $U=8t$ and $4t$, leading to $J=t/8$ and $t/4$. For a more realistic $J=t/8$, the extrapolated energies for the *C*-AF and CE phases

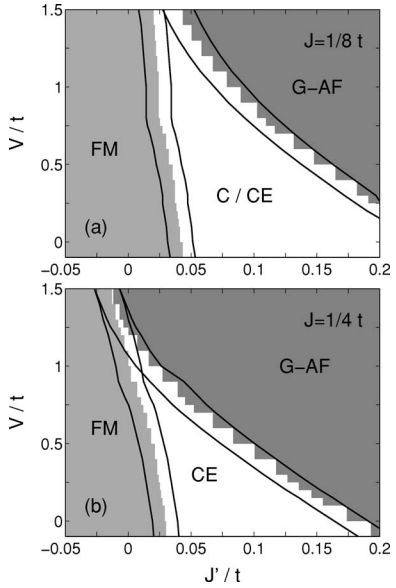

FIG. 13. Phase diagram at half doping $(x=0.5)$ for (a) $J=0.125t$ and (b) $J=-.25t$, as obtained from finite-size considerations at orbital degeneracy $(E_z=0)$. The black lines around the phase boundaries give their estimated numerical and finite-size errors. At $J/t=1/8$ the energies for the *C*-AF and CE phases differ only *very little* and we could not determine a phase boundary between them. For $J/t=1/4$ the CE phase has lower energy than the *C*-AF phase.

are indeed very close to each other, with $V>0$ slightly favoring the CE phase (see above), and we anticipate that the observed differences might actually be smaller than the error induced by the use of 1D chains instead of 2D clusters. We therefore could not determine a phase boundary between these two phases. We also had to compare the energies of the two quasi-1D phases to the 2D-like FM and AF phases. However, we observed that the energy of the CE phase for $L=8$ is already very similar to the extrapolated result for $L\rightarrow\infty$ for all values of V. Therefore the results obtained for the 8×2 cluster [see Fig. 7(c)] could be used for energy comparison with the FM and AF phases.

In order to estimate the uncertainty of the ground-state energies in a reliable way and, thus, of the determined phase boundaries, we further investigated the change of the energy of the FM phase with cluster size for three clusters used in the present calculations: $\sqrt{8}\times\sqrt{8}$, $\sqrt{10}\times\sqrt{10}$, and 4×4. It was found that the energies did not depend much on cluster size, but these might, however, still be too small. A somewhat simpler situation occurs for the *G*-type AF phase which turns out to be perfectly charge ordered for $V\gtrsim-J$, so its energy is independent of V. Moreover, as all electrons are perfectly localized, one finds in the present approximation a classically ordered *G*-AF phase without finite-size effects.

For the *C*-AF and CE phases, we investigated how much the energy of the CE phase for $L=8$ differs from the extrapolated energies for either the *C*-AF or the CE phase at $L\rightarrow\infty$. We finally arrived at the estimated error $\Delta J'\leqslant\frac{\Delta E}{2}\approx0.01t$ and the resulting phase diagram for $J/t=1/8$ given in Fig. 13(a). The CE or *C*-AF phases are stable in between the AF and FM phases, respectively. Increasing nearest-

neighbor Coulomb repulsion $V>0$ weakly suppresses the FM phase and favors the AF phase. On the one hand, the FM phase is suppressed because it is stabilized by the kinetic energy which decreases when the charge order is induced by finite V. The AF phase, on the other hand, is already charge ordered in the absence of explicit Coulomb repulsion and is therefore not influenced by V. Altogether, the electrons redistribute at finite V also in the CE phase, so its range shrinks.

For a smaller on-site Coulomb repulsion $U=4t$—e.g., $J/t=1/4$—the CE phase is favored over the C phase for all values of V, at least in the investigated parameter range $-0.5t \leqslant V \leqslant 2t$. We used the same procedure as described above to determine the boundary toward the FM and AF phases, and arrived at the phase diagram depicted in Fig. 13(b). One finds that the G-AF phase extends to a broader range of parameters, and the region of CE phase is reduced with increasing V. This contradicts the common belief that the CE phase is stabilized by the nearest-neighbor Coulomb interaction.

E. Magnetic and orbital correlations for increasing doping

We complete this section by a qualitative discussion of the changes in orbital occupation and magnetic correlations in a monolayer under increasing doping. For a 4×4 cluster doped with one hole ($x=1/16=0.0625$) we observed rather weak AF order in MC runs for $J'=0.02t$ and more pronounced AF order for $J'=0.05t$, with $E_z=V=0$. Unfortunately, we were not able to perform MC simulations for more than one hole on 4×4 clusters ($x>1/16=0.065$) due to the increasing size of the Hilbert space. For one hole doped to a smaller $\sqrt{8}\times\sqrt{8}$ cluster (doping $x=1/8=0.125$), we found weakly AF correlations for $J'=0.05t$, while AF order had vanished for $J'=0.02t$, which is a clear sign of the increasing importance of FM double exchange with increasing doping. The fast disappearance of AF order ($x\gtrsim0.125$ for $J'=0.02t$) agrees with experimental observations, where AF order disappears at $x\gtrsim0.115$ and is replaced by short-range spin-glass type of order.[10]

Magnetic correlations at higher doping are theoretically challenging, and various anisotropic magnetic phases (A-AF and C-AF) were obtained in the model discarding strong Coulomb repulsion.[35] In the range of large doping $x>0.5$, higher doping can be reached for $Nd_{1-x}Sr_{1+x}MnO_4$, while $La_{1-x}Sr_{1+x}MnO_4$ can be doped only up to $x\approx0.7$. In $Nd_{1-x}Sr_{1+x}MnO_4$ samples the C-AF phase was observed[60] for $0.75<x<0.9$; additionally, a structural phase transition suggesting predominant occupation of directional orbitals along one axis was reported. We found it very encouraging that the same trends have been observed in the MC simulations for two electrons on a $\sqrt{8}\times\sqrt{8}$ cluster and for four electrons on a 4×4 cluster ($x=3/4$), as well as for three electrons on 4×4 cluster ($x=0.8125$), for large enough $J'=0.025t$ and $0.05t$.

The spin correlations obtained from MC simulations of a $\sqrt{8}\times\sqrt{8}$ cluster with two electrons are shown in Fig. 14 for two parameter sets $J'=0.05t$, $V=E_z=0$ and $J'=0.025t$, $V=t$, $E_z=0.25t$. For a larger value of $J'=0.05t$ we see the telltale signal of the C-type phase, the strongly negative signal at

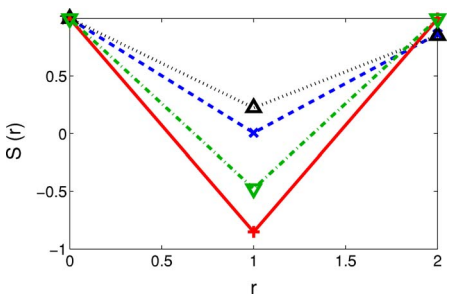

FIG. 14. (Color online) MC results for the spin-spin correlations $\mathcal{S}(\vec{r})$, Eq. (26), for a monolayer, as obtained in $\sqrt{8}\times\sqrt{8}$ cluster with two electrons (at high $x=0.75$ doping) for two parameter sets $J'=0.05t$, $V=0$, $E_z=0$ [$\times$ for (10) and $+$ for (11) direction] and $J'=0.025t$, $V=t$, $E_z=0.25t$ [$\triangle$ for the (10) and $\triangledown$ for the (11) direction]. Error bars are smaller than symbol sizes. Parameters: $J=0.125t$, $\beta t=100$.

(11). The nearest-neighbor spin correlation in the (10) direction nearly vanishes because the FM and AF signals from the two directions almost cancel each other. (Parallel tempering was employed in this case to ensure good autocorrelation times.) For smaller $J'=0.025t$ and $V=t$, $E_z=0.25t$, the C-AF phase is not as marked and the FM correlations are stronger than the AF ones. In agreement with expectations based on the 1D model,[20] the electrons occupy directional orbitals along the FM direction in the C-AF phase, because this maximizes the gain of the kinetic energy.

Figure 15 shows that orbital occupation depends strongly on doping for realistic parameters $J'=0.025t$ and $V=t$. This is reflected by the percentage of electrons occupying out-of-plane $|z\rangle$ orbitals which is furthermore very sensitive to the actual value of E_z (see Fig. 15). It is quite remarkable that for the degenerate e_g orbitals—i.e., without a crystal field ($E_z=0$)—practically only in-plane $|x\rangle$ orbitals are occupied at $x=0$ [squares in Fig. 15(a)]. This state is induced by finite AF superexchange $J'=0.025t$ which (due to large Hund's exchange) selects the AF interactions between e_g, and these interactions are maximal in ab planes when $|x\rangle$ orbitals are occupied. In this way the core-spin superexchange influences also the e_g orbital occupation (at $J'=0$ one finds an almost isotropic electron distribution with $n_z/n\simeq0.5$ in the FM phase). Upon doping, the electron population in $|z\rangle$ orbitals gradually increases, reaches a maximum at $x=5/8$ where FM correlations are found, and then decreases again. This behavior follows from the kinetic energy which contributes in the entire regime of $0<x<1$ and is gained when the interorbital processes which excite electrons to $|z\rangle$ orbitals, $\sim\sqrt{3}(\tilde{c}^{\dagger}_{ix}\tilde{c}_{jz}+\tilde{c}^{\dagger}_{iz}\tilde{c}_{jx})/4$, are allowed.

For a large positive crystal field favoring $|z\rangle$ orbitals $E_z=0.5t$ [triangles in Fig. 15(a)], the density distribution is reversed at $x=0$—almost all electrons are found within $|z\rangle$ orbitals. They redistribute, however, gradually with increasing doping, because the kinetic energy competes with the crystal field and favors in-plane $|x\rangle$ orbitals. (In this case one finds a FM phase in a range of doping from $x=1/4$ to $x=5/8$, separated by the CE phase found at $x=0.5$ for $E_z=0$.) In the intermediate case of a smaller crystal-field splitting of $E_z=0.2t$ (crosses), the normalized $|z\rangle$ density n_z/n is first re-

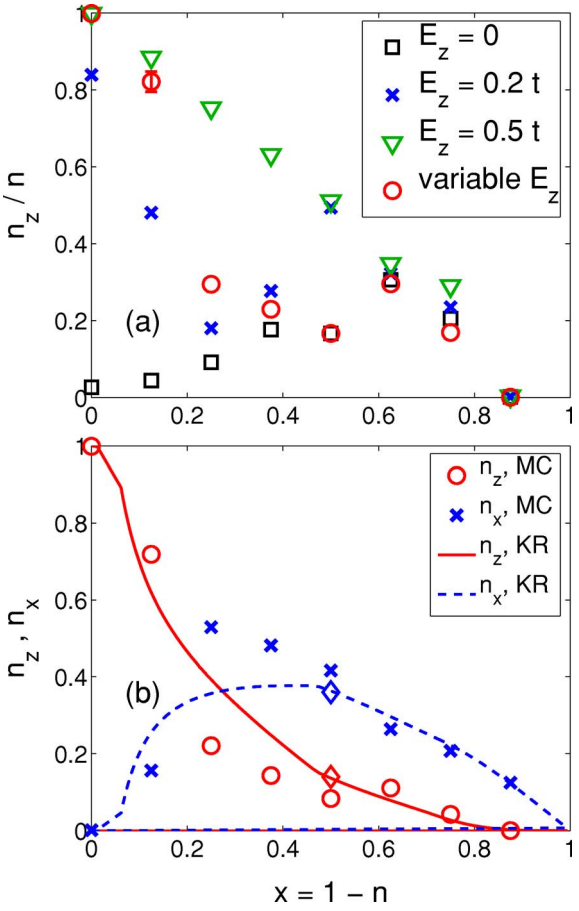

FIG. 15. (Color online) Orbital electron densities for increasing doping $x=1-n$ as obtained in MC method for a $\sqrt{8}\times\sqrt{8}$ cluster: (a) percentage of density in $|z\rangle$ orbitals n_z/n for a few selected values of the crystal-field parameter E_z and for variable E_z (see below) and (b) absolute densities n_z and n_x in the two orbitals from MC (symbols) compared with the densities found with the Kotliar-Ruckenstein (KR) slave-boson mean-field approximation Ref. 61 (lines) with variable $E_z=(\frac{1}{2}-x)t$. The charge distribution found at doping $x=0.5$ with the KR method ($n_z\simeq 0.14$, $n_x\simeq 0.36$) is indicated by diamonds. Remaining parameters in the MC calculations: $J=0.125t$, $J'=0.025t$, $V=t$, $\beta t=100$.

duced but next rises again towards the FM phase which in this case suppresses the CE phase at $x=0.5$.

As in the last scenario, we investigated the effect of a doping-dependent crystal-field splitting,

$$E_z=\left(\frac{1}{2}-x\right)t. \tag{35}$$

The doping dependence of this type [circles in Fig. 15(a)] is qualitatively expected by considering the experimental data.[8] This is probably the most realistic case of those considered here, as it shows both the correct orbital polarization for $x=0$ and the CE phase for $x=0.5$. Note that in all cases except $E_z=0$, we find the experimentally observed[8] increase of in-plane $|x\rangle$ electron density with increasing doping which shows that $E_z>0$ in the low-doping regime.

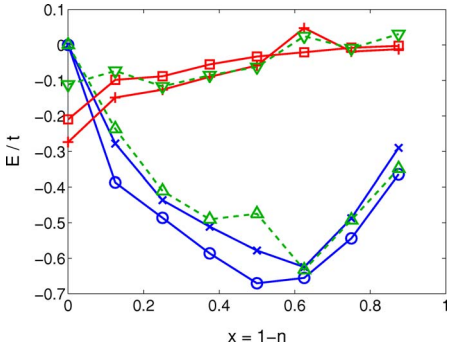

FIG. 16. (Color online) Kinetic (approximately parabolic shape) and superexchange (weakly increasing) energies for increasing doping $x=1-n$, as obtained for $\sqrt{8}\times\sqrt{8}$ clusters with various parameter sets: ○ and □, for $J'=0$ and $E_z=V=0$; × and +, for $J'=0.05t$ and $E_z=V=0$; △ and ▽, for $J'=0.025t$, $V=t$, and E_z given by Eq. (35). Parameters: $J=0.125t$, $\beta t=100$.

Taking the decreasing with x crystal field as in Eq. (35), one finds a very fast decrease of n_z from $n_z=1$ at $x=0$ to $n_z\simeq 0.22$ at $x=0.25$ [Fig. 15(b)]. Thus the electrons move fast from $|z\rangle$ to $|x\rangle$ orbitals in this doping regime, as dictated by the kinetic energy gain. This qualitative trend is very well reproduced by the analytic approach using the mean-field approximation in the slave-boson method, introduced by Kotliar and Ruckenstein.[61] We have adapted this method to the FM phase in a monolayer, as explained in the Appendix. The performed comparison with the results of exact diagonalization shows that this analytic approach provides a surprisingly reliable way to estimate both the charge distribution in layered systems and the magnetic interactions at increasing doping. In the present case the double-exchange mechanism promotes FM states in a large range of doping, while in a bilayer system changing the electron density distribution provides a natural explanation for an observed transition from the FM to A-AF structure.[15]

The changes in magnetic correlations at increasing doping follow from the competing superexchange and double-exchange interactions. The double exchange is directly proportional to the kinetic energy,[34] which vanishes at $x=0$ and is gradually gained by doping when the available space for hopping processes increases up to $x\sim 0.5$ and then is gradually lost beyond half doping (see Fig. 16). Therefore, the kinetic energy has an approximately parabolic shape, as obtained for a $\sqrt{8}\times\sqrt{8}$ cluster with a few representative parameter sets. Since different orbital occupations can favor either the FM or AF spin configuration for any bond, the superexchange energy is finite even in the cases where the average nearest-neighbor spin correlation function vanishes, like in the CE and C-AF phases.

In the FM case at $J'=0$, the kinetic energy has its minimum at $x=0.5$ because of the optimal carrier density (Fig. 16). For $J'>0$, however, the minimum of the kinetic energy is moved to larger doping $x=5/8=0.625$, because this electronic filling allows one to realize the FM phase, while the magnetic correlations favor instead the CE phase at $x=0.5$ at the expense of the kinetic energy. This demonstrates that these two energies are to some extent complementary and their competition controls the magnetic order. With finite

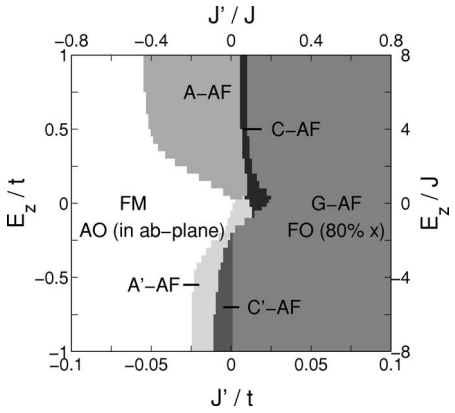

FIG. 17. Phase diagram of the undoped bilayer system as obtained in the (E_z, J') plane with a $\sqrt{8}\times\sqrt{8}\times 2$ cluster at $T=0$. The phases found between FM and G-AF order for two ab planes with interlayer coupling along the c axis are C-AF and A-AF phases as in Fig. 1, C'-AF: FM along the c axis and AF within the ab planes, A'-AF: FM along the a and c axes, and AF along the b axis. The OO which accompanies the FM and G-AF phase at $E_z=0$ is also indicated and shown in Figs. 18(a)–18(c). Units J'/t and E_z/t correspond to $J=0.125t$.

nearest-neighbor Coulomb repulsion $V=t$, the kinetic energy of the CE phase is partly lost due to charge order. Concerning the total energy, which contains additional contributions from V and E_z and is not shown in Fig. 16, we want to emphasize that it is convex over the entire doping range and for all parameter sets. Although this result seems to exclude phase separation,[22] the clusters used in the present study are definitely too small to address this issue in a conclusive way.

IV. MAGNETIC PHASES IN BILAYER MANGANITES

A. Phase diagrams for undoped system

Bilayer manganites like $La_{2-2x}Sr_{1+2x}Mn_2O_7$ represent an intermediate situation between the 2D monolayer systems and 3D perovskite manganites, so it is interesting to ask to what extent the qualitative trends reported above for the monolayers are modified by the interlayer coupling. We shall provide some limited answers to this question, as unfortunately the calculations could only be performed for certain selected fillings of the smallest bilayer $\sqrt{8}\times\sqrt{8}\times 2$ cluster used in the numerical studies.

The study of magnetic correlations in an undoped ($x=0$) system performed on $\sqrt{8}\times\sqrt{8}\times 2$ clusters led to the phase diagram in the (J', E_z) plane (see Fig. 17). It was obtained by comparing the energies of various possible magnetic states at $T=0$. As in a monolayer, large positive J' leads to the G-AF phase (with AF correlations in all three spatial directions) and strongly negative J' induces FM phase.[40] Apart from these two phases, one finds here several different types of intermediate magnetic order in the crossover regime from the FM to G-AF phase, with FM bonds along either two or only one cubic direction (see Fig. 1). Two phases of the same type, either A-AF and A'-AF or C-AF and C'-AF, are distinguished by the directions of FM bonds. When the FM correlations occur within the ab layers, as found experimentally,[12] they are called A-AF and C-AF phases, respectively. These phases appear for the expected[13] positive ($E_z>0$) crystal field which favors $|z\rangle$ orbital occupancy, while for the $E_z<0$ interlayer FM correlations occur in A'-AF and C'-AF phases.

For intermediate J', one obtains the A-AF phase, reminiscent of the ground state of undoped 3D perovskite manganite $LaMnO_3$. For $E_z \gtrsim 0.2t$ this plane is particularly robust, which suggests that positive E_z simulates here the effect of missing planes along the c axis on the electron distribution. A large-$|z\rangle$ amplitude is needed as (i) this type of order is supported by the AO order in the ab planes and (ii) $|z\rangle$ orbitals are responsible for the AF interlayer coupling. This coexisting AO-FM phase within the ab planes is robust and can be suppressed only by AF core-spin superexchange $J'>0$ of a similar value as in the monolayer (see Fig. 2).

MC simulations performed at $\beta t=100$ for various parameter sets support the phases found in the ground-state calculations ($J=t/8$ in all cases): $J'=0.05t$, $E_z=0$ (G-AF); $J'=-0.02t$, $E_z=0$ (FM); $J'=0$ and $J'=-0.02t$, $E_z=0.5t$ (A-AF); $J'=-0.005t$, $E_z=-0.5t$ (C'-AF). For some parameter sets close to the ground-state phase boundaries, we observe competing phases; i.e., configurations showing several different phases occur in the MC runs: $J'=0$, $E_z=0$ (FM and A-AF) and $J'=0.01t$, $E_z=0$ (A-AF, some configurations with A'-AF and C-AF).

The crossover region from the FM to the G-AF phase with increasing J' is characterized by the competition between nearly degenerate magnetic phases. As for the monolayer phase diagram, the ground-state calculations also yield small regions with the C-AF or C'-AF phases. The C'-AF was indeed found in MC runs for $J'=-0.005t$, $E_z=-0.5t$, $\beta t=100$, and $J=1/8t$, but the C-AF phase (having a very narrow stability region in the ground-state phase diagram) only occasionally surfaced in the MC runs for $E_z=0$ and $J'=0.01t$ (competing with A-AF) and $J'=0.02t$ (competing with G-AF). It also occasionally occurs at $J'=0.015t$, but the magnetic structure there remains unclear, which could mean that temperature was still too high and/or the cluster too small.

For negative E_z in-plane $|x\rangle$ orbitals are favored, which in turn enhances the region of stability of the G-AF phase. This can be understood by looking at the orbital correlations in the G-AF phase at $E_z=0$ depicted in Fig. 18(a): Even at orbital degeneracy (without a crystal field), one finds rather pronounced polarization for $\theta=0-80\%$ of the electrons occupy $|x\rangle$ orbitals as then the superexchange energy is gained. The G-AF phase can therefore take advantage of a negative E_z, as seen in the phase diagram of Fig. 17.

Figure 18(b) shows the orbital correlations in the FM phase, where strong AO order within the layers coexists with FM order in the ab planes. As this AO order can best develop when occupations of $|x\rangle$ and $|z\rangle$ orbitals are nearly equal, the FM phase is most pronounced around $E_z=0$. At the same time, the interlayer coupling (kinetic energy) is much weaker. This state competes with the G-AF state with larger occupancy of $|x\rangle$ orbitals.

Finally, the A-AF phase is found mainly for $E_z>0$ which enhances the electron density in $|z\rangle$ orbitals and supports the AF interlayer coupling. The orbital correlations in this phase

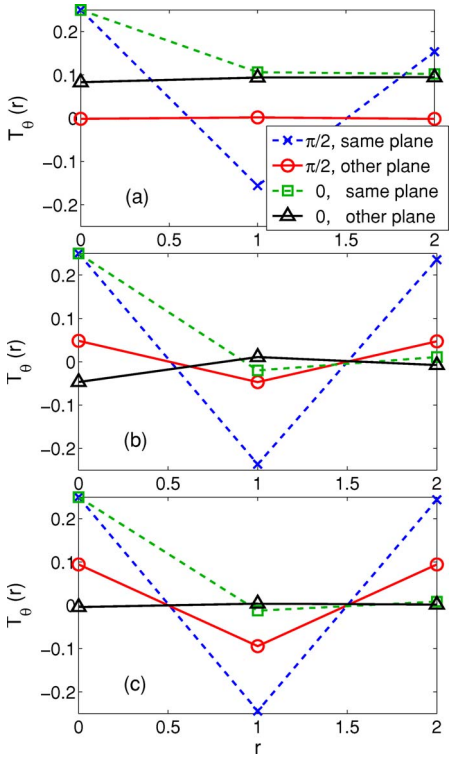

FIG. 18. (Color online) Orbital correlations $\mathcal{T}_\theta(\vec{r})$ (27) in the (01) direction within one *ab* plane and between the two different planes of the bilayer, as obtained for the undoped $\sqrt{8}\times\sqrt{8}\times 2$ clusters at $E_z=0$ and $T=0$ in the (a) *G*-AF phase, (b) FM phase, and (c) *A*-AF phase. In each case T_i^z operators are defined by different bases of orthogonal orbitals: $\theta=0$—$\{|x\rangle,|z\rangle\}$ and $\theta=\pi/2$—$\{|x\rangle+|z\rangle,|x\rangle-|z\rangle\}$. Parameters: (a) $J'=0.05t$; (b) and (c) $J'=-0.02t$.

(at $E_z=0$) are depicted in Fig. 18(c)—one finds the AO order within the FM planes; i.e., orbital correlations for $\theta=\pi/4$ are strongly alternating within the *ab* planes. Between the planes—i.e., along the AF bonds in the *c* direction—the orbital correlation is weakly positive, indicating weak FO order.

Although the phase diagram of Fig. 17 was obtained with small $\sqrt{8}\times\sqrt{8}\times 2$ clusters, we argue that it is representative of the bilayer system in the thermodynamic limit, as it is determined by short-range spin and orbital correlations that follow from local superexchange interactions (charge excitations) on the nearest-neighbor bonds. To support this point of view we present also the phase diagram found with a smaller $2\times 2\times 2$ cluster in Fig. 19. One finds that indeed the same phases occur as in Fig. 17 and their stability regimes are remarkably close to those of the larger $\sqrt{8}\times\sqrt{8}\times 2$ cluster.

B. Competition between different phases in half-doped bilayer clusters

Next, we investigate the magnetic and orbital order at half doping, assuming orbital degeneracy ($E_z=0$). Figure 20(a) shows the energy of various phases of the half-doped bilayer depending on the value of the t_{2g} superexchange J' in the absence of intersite Coulomb repulsion ($V=0$). Not only for negative but also for small positive J', the system is FM,

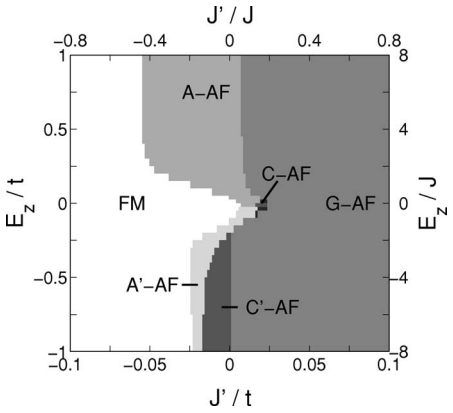

FIG. 19. Phase diagram of the undoped $2\times 2\times 2$ cluster as obtained in the (E_z,J') plane at $T=0$. The phases and parameters are the same as in the bilayer system (Fig. 17), with the directions of FM bonds in *A*-AF, *A'*-AF, and *C'*-AF phases distinguished by the symmetry-breaking crystal field $\propto E_z$ [see Eq. (11)]. The *C*-AF phase almost vanishes in this case.

while for larger positive $J'>0.02t$ one finds the *G*-AF phase. In between these phases the CE phase, with alternating FM zigzag chains in the *ab* planes and AF coupling between them, has a lower energy. However, finite-size effects are again important, as discussed in Sec. III B, and thus one expects that instead the *C*-AF phase is the actual ground state in the thermodynamic limit for the present realistic parameters. (Similar to the 1D chains used for finite-size consider-

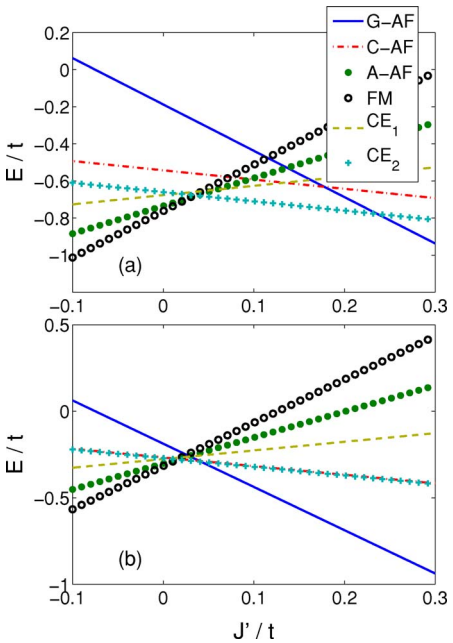

FIG. 20. (Color online) Ground-state energy *E* of various magnetic phases for increasing t_{2g} superexchange J' in the half-doped bilayer $\sqrt{8}\times\sqrt{8}\times 2$ cluster, as obtained at $T=0$ for (a) $V=0$ and (b) $V=t$. Different phases with coexisting AF and FM bonds are defined as follows: *C*-AF, FM in the *a* direction; *A*-AF, AF in the *c* directions, FM in the *ab* planes; CE_1, FM zigzag chains in the *ab* planes with FM interlayer coupling; CE_2, FM zigzag chains in the *ab* planes with AF interlayer coupling. Parameters: $J=0.125t$, $E_z=0$.

ations instead of 2D clusters, one can use 2D ladderlike clusters instead of 3D clusters, but as the attainable lengths are here much shorter definite results are difficult to obtain. However, an energy comparison of the C-AF and CE phases on 4×2 and 8×2, including 6×2 for the C-AF phase, suggests that the C-AF phase has lower energy.)

We have already shown in the case of a monolayer that the nearest-neighbor Coulomb repulsion V decreases the range of stability of the CE phase. Also for the bilayer system the CE phase is suppressed by $V\sim t$, with weak preference for the C-AF phase [Fig. 20(b)]. Namely, one finds that the energy of the C-AF phase is lower than that of the CE phase for $V=t$ and $J'>0.02t$. The reason is that the interlayer charge stacking (along the c direction) required by the CE phase costs extra energy now, whereas the C-AF phase permits alternating charge order in all three directions and has thus a lower energy-increment due to V. Unlike for the 2D clusters of Sec. III D, the situation here is also similar for $J=0.25t$ (not shown). We have verified that both phases here have very similar energies on an 8×2 ladder, which seems to indicate that the C-type phase wins in the thermodynamic limit for $J=t/4$ as well. For $V=t$ and $J'<0.02t$ the A-AF phase is more stable than the CE phase, which suggests that this parameter range is relevant for the experimentally measured $LaSr_2Mn_2O_7$ sample.[11,12]

However, isotropic magnetic phases, FM for $J'<0.02t$ and G-AF for $J'>0.02t$, are more stable than anisotropic phases in the entire range of J' if $V=t$ [Fig. 20(b)]. As for monolayers, finite $V>0$ favors the G-AF phase, because its kinetic energy vanishes already for $V=0$ and thus the energy of this phase is not affected by V, while charge order induced by V in other phases hinders electron motion, and thus their total energies increase. While the spin-orbital model leads to the CE phase in a monolayer at $J\gtrsim t/8$ or for $V>0$, lattice degrees of freedom are apparently needed to stabilize it in 3D perovskites. Furthermore, it should be noted that the bilayer compound $LaSr_2Mn_2O_7$ shows A-AF order,[11,12] in contrast to the monolayers and the 3D compounds. The origin of this behavior remains unclear at present, especially as the orbital correlations are reported to be similar in all cases.[10,16]

C. Bilayer clusters at large doping

The reference system for large hole doping regime is $x=1$ case, when itinerant e_g electrons are absent and the magnetic order depends exclusively on core spin superexchange J'—one finds then the G-AF phase for $J'>0$ (while an unphysical $J'<0$ induces the FM phase). We have been able to investigate the highly doped regime because the small number of electrons leads here to a small Hilbert space which allows us to perform MC simulations down to $x\geqslant3/4$ on a $\sqrt{8}\times\sqrt{8}\times2$ cluster (filled by up to 4 electrons). MC simulations show that G-AF order for $J'=0.05t$ is strong enough to persist upon inclusion of one e_g electron—i.e., at doping $x=15/16$—as demonstrated by spin correlations presented in Fig. 21(a). They describe G-type alternating spin order in all three directions.

Somewhat lower doping $x=13/16$ (three electrons in the present cluster) gives a C-AF phase with FM chains lying in the ab planes and predominant occupation of directional orbitals along the FM direction—this state is stabilized by the double-exchange mechanism. Indeed, the strongly negative spin correlation at the (1,1) point [see Fig. 21(b)] is a signature of the C-AF phase. For distance $r=1$ along the (0,1) direction, the signal is approximately zero, because the FM and AF correlations in the two directions nearly cancel each other. Finally, the intermediate case of $x=0.875$ (with two electrons) does not allow to establish a clear picture of magnetic correlations (not shown), which may be due to strong competition between the two AF phases. In fact, experiments show a transition from G-AF to C-AF at doping $x\approx0.9$ (see Ref. 12) which agrees with these results.

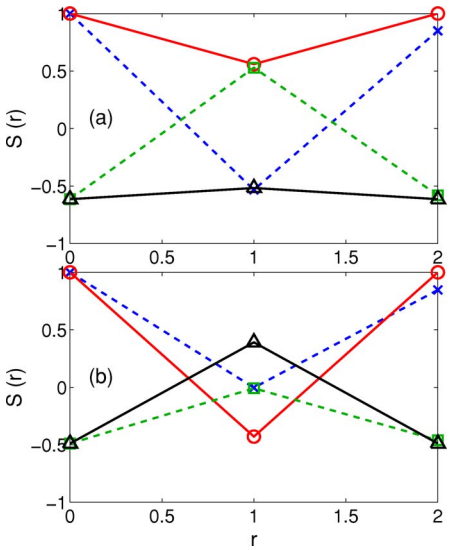

FIG. 21. (Color online) Spin correlations (26) as obtained from MC simulations with a $\sqrt{8}\times\sqrt{8}\times2$ cluster in the highly doped regime for increasing coordinate r in the ab plane: (a) G-AF phase for one electron ($x=15/16$) and (b) C-AF phase for three electrons. Different symbols and lines indicate different types of neighbors: × and dashed (blue) line, within the ab planes along either the (01) or (10) direction; ○ and solid (red) line, within the ab planes along the (11) direction; □ and dashed (green) line, between the two planes along the a or b direction; △ and solid (black) line, between the two planes and along the (11) direction in the ab plane. Parameters: $J=0.125t$, $J'=0.05t$, $V=E_z=0$, $\beta t=100$.

V. DISCUSSION AND CONCLUSIONS

The present study clarifies that orbital degrees of freedom are of crucial importance for the understanding of magnetic correlations in layered manganites. We treated a realistic model including intraorbital and interorbital Coulomb interactions and investigated charge, intersite spin, and intersite orbital correlations in monolayer and bilayer manganites. The obtained results revealed a close relationship between orbital and magnetic order which follows the Goodenough-Kanamori rules at $x=0$.[42] The magnetic phases found in different doping regimes, where double exchange also contributes, are in accordance with experiments over the whole doping range $0\leqslant x\leqslant1$, particularly for the monolayer systems.

For the undoped monolayers the model predicts either FM or AF order, but not the *E*-AF phase, reported previously in an approach similar to ours but ignoring on-site Coulomb repulsion between the e_g electrons.[22,23] In their study it was stabilized by the kinetic energy and arose mainly for *nearly vanishing* electron-phonon coupling[23] i.e., in the situation when lattice degrees of freedom could be neglected. Otherwise, the model of Ref. 23 is similar to our Hamiltonian apart from missing Coulomb repulsion. Experimentally, however, the *E*-AF phase is only observed[43] for the very *strongly* JT-distorted $HoMnO_3$ and never in less distorted compounds. In the FM phase, the OO induced by the orbital superexchange—i.e., by local Coulomb repulsion—is found even in the absence of electron-phonon coupling, in contrast to the model without Coulomb repulsion.[23] This shows that the correct treatment of electron correlation effects due to large Coulomb repulsion, which suppresses the kinetic energy in undoped compounds (at $x=0$), is crucial for the qualitatively correct description in this doping regime.

The experimental situation in doped $La_{1-x}Sr_{1+x}MnO_4$ could be modeled with varying crystal fields favoring out-of-plane $|z\rangle$ orbitals in the undoped system and gradually decreasing with x to accelerate the electron transfer from $|z\rangle$ to $|x\rangle$ orbitals. Indeed, for positive $E_z \sim 0.5t$ the undoped monolayers contain then almost only $|z\rangle$ electrons, while the $|x\rangle$ occupation grows rapidly with doping when E_z decreases in the present model (see Fig. 15 in Sec. III E). Indeed, such a doping dependence of E_z is suggested by recent experiments.[8]

Another success of the model is that one observes the CE phase at half doping with physically realistic parameters for layered manganites; i.e., it is obtained for small t_{2g} superexchange $J' \gtrsim 0.03t$, as deduced[29] from the analysis of exchange constants in $LaMnO_3$. We also investigated the impact of nearest-neighbor Coulomb repulsion and found it to *slightly* stabilize the CE phase with respect to the *C*-AF phase in monolayers in the relevant regime of J', but to favor instead the *C*-AF phase in bilayer clusters. (In both cases, the stability region of either the CE or *C*-AF phase shrinks and that of the *G*-AF phase grows when nearest-neighbor Coulomb repulsion is included.) In the CE phase, we found relatively similar electron densities at corner ($n^c \simeq 0.413$) and bridge ($n^b \simeq 0.587$) positions in the zigzag FM chains, which clearly contradicts the localized picture of this phase. Furthermore, we observed that electrons occupy mainly bridge positions; they are found in the directional $3x^2-r^2/3y^2-r^2$ orbitals without crystal field, and in the planar z^2-x^2/y^2-z^2 orbitals for the $E_z>0$. While this is in contrast to the interpretation of some experiments,[51,52] other groups reported a similar charge distribution.[55] It is quite remarkable, however, that the CE phase could be here explained by a purely electronic mechanism—one may expect that the oxygen distortions due to the JT effect would further stabilize it. Also, at large doping , the calculations for monolayer clusters predict the *C*-AF phase with predominant occupation of directional orbitals, in agreement with experimental data for $Nd_{1-x}Sr_{1+x}MnO_4$.[60]

An interesting variation of spin and orbital correlations with doping was also found in the bilayer systems. They can be considered as intermediate between 2D and 3D manganites, and we obtained the *A*-AF phase for the realistic parameters at $x=0$, observed in undoped 3D $LaMnO_3$ perovskite compound. The absence of the CE phase in the bilayer phase diagram of Ling *et al.*[12] could not be explained, however. Perhaps the electron transfer from $|z\rangle$ to $|x\rangle$ orbitals at increasing doping is really fast, as suggested by the variation of intralayer and interlayer exchange constants,[15,17] and then the *A*-AF phase is stabilized again, yet by different physical mechanisms. For very large doping $x>0.75$, however, we obtained the *C*-AF and *G*-AF phases with a transition between them, as indeed observed in bilayer compounds.[12]

Summarizing, the present study shows that the internal frustration of magnetic interactions in doped manganites, with competing FM/AF terms in the spin superexchange which coexist with complementary terms in the orbital superexchange, has important consequences. Due to the intricate energy balance between different types of intersite correlations, the magnetic order may be completely switched over by small changes of microscopic parameters, when the orbital order which coexists with it switches at the same time. We find it quite encouraging that these generic features, as well as the experimentally observed trends in layered manganites, could be reproduced within the present microscopic model.

ACKNOWLEDGMENTS

We thank C. Baumann, B. Büchner, P. Horsch, and R. Klingeler for insightful and stimulating discussions. This work has been supported by the Austrian Science Fund (FWF), Project No. P15834-PHY. A.M.O. would like to acknowledge support by the Polish Ministry of Science and Education under Project No. 1 P03B 068 26, and by COST Action P16, ECOM.

APPENDIX: SLAVE-BOSON APPROACH FOR THE 2D MODEL OF SPINLESS FERMIONS

It is notoriously difficult to implement electron correlation effects in the nonmagnetic phases realized in multiband models. Therefore we consider here a simpler case of a FM monolayer in the limit of large $U\rightarrow\infty$ to compare the resulting charge distribution with the exact diagonalization of finite 2D clusters. The electronic structure for e_g electrons is then described by the so-called orbital Hubbard model of Ref. 21.

It was shown recently[21] that cubic invariance is obeyed when the constraint of no double occupancy in the limit of large U is implemented by slave bosons for electronic states, using a basis of complex orbitals at each site i,

$$|+\rangle_i = \frac{1}{\sqrt{2}}(|z\rangle_i - i|x\rangle_i), \quad |-\rangle_i = \frac{1}{\sqrt{2}}(|z\rangle_i + i|x\rangle_i). \quad \text{(A1)}$$

Then the hopping term H_t^{2D}, Eq. (14), and the crystal-field term H_z, Eq. (11), may be written as follows (the superexchange terms vanish in the limit of $U\rightarrow\infty$):

$$H_t^{U=\infty} = -\frac{1}{2}t \sum_{\langle ij\rangle \| a,b} [c_{i+}^\dagger c_{j+} + c_{i-}^\dagger c_{j-} + (e^{-i\chi_\alpha} c_{i+}^\dagger c_{j-} + e^{+i\chi_\alpha} c_{i-}^\dagger c_{j+}) + \text{H.c.}] - \frac{1}{2}E_z \sum_i (c_{i+}^\dagger c_{i-} + c_{i-}^\dagger c_{i+}), \quad \text{(A2)}$$

where $c_{i\pm}^\dagger$ are the corresponding creation operators and $\chi_a = +2\pi/3$ and $\chi_b = -2\pi/3$ are the phase factors for the bonds $\langle ij\rangle$ along the a and b axes. Note that the crystal-field term contains only off-diagonal terms for the complex orbital stares (A1). In order to implement rigorously the constraint at $U=\infty$ we replace now the fermion operators as follows:

$$c_{i\pm}^\dagger = b_{i\pm}^\dagger f_{i\mp}^\dagger e_i, \quad \text{(A3)}$$

corresponding to a representation of the local states by

$$|0\rangle_i = e_i^\dagger |\text{vac}\rangle,$$

$$|+\rangle_i = c_{i+}^\dagger |0\rangle_i = b_{i+}^\dagger f_{i-}^\dagger |\text{vac}\rangle,$$

$$|-\rangle_i = c_{i-}^\dagger |0\rangle_i = b_{i-}^\dagger f_{i+}^\dagger |\text{vac}\rangle, \quad \text{(A4)}$$

where $|\text{vac}\rangle$ is a true vacuum, following Ref. 21. In the slave-boson mean-field approximation we replace the boson operators by their averages, which leads to the (*a priori* site-dependent) hopping renormalization factors $q_{i\pm}$. For an isotropic charge distribution one finds then, from a global constraint

$$n_+ + n_- = 1 - x, \quad \text{(A5)}$$

that the renormalization factors

$$q_{i\pm} = \frac{x}{1 - \langle f_{i\mp}^\dagger f_{i\mp}\rangle} = \frac{x}{1 - \langle n_\pm\rangle} = q_\pm \quad \text{(A6)}$$

are the same for all kinetic energy terms. In this way one arrives at the effective Hamiltonian with renormalized hopping terms

$$\mathcal{H}_{U=\infty}^{\text{MF}} = -\frac{1}{2}t \sum_{\langle ij\rangle \| a,b} [q_+ \hat{f}_{i+}^\dagger \hat{f}_{j+} + q_- \hat{f}_{i-}^\dagger \hat{f}_{j-} + \sqrt{q_+ q_-}(e^{-i\chi_\alpha} \hat{f}_{i+}^\dagger \hat{f}_{j-} + e^{+i\chi_\alpha} \hat{f}_{i-}^\dagger \hat{f}_{j+}) + \text{H.c.}] - \frac{1}{2}E_z \sum_i (\hat{f}_{i+}^\dagger \hat{f}_{i-} + \hat{f}_{i-}^\dagger \hat{f}_{i+}). \quad \text{(A7)}$$

By diagonalizing it in reciprocal space and using the inverse transformation to Eq. (A1),

$$|z\rangle_i = \frac{1}{\sqrt{2}}(|+\rangle_i + |-\rangle_i), \quad |x\rangle_i = \frac{i}{\sqrt{2}}(|+\rangle_i - |-\rangle_i), \quad \text{(A8)}$$

we determined the occupations of $|x\rangle$ and $|z\rangle$ orbitals shown in Fig. 15(b). A similar analysis used before for the bilayer system gave the density distribution and the effective exchange constants in good agreement with experiment.[15]

[1] G. H. Jonker and J. H. van Santen, Physica (Amsterdam) **16**, 337 (1950).

[2] R. von Helmolt, J. Wecker, B. Holzapfel, L. Schultz, and K. Samwer, Phys. Rev. Lett. **71**, 2331 (1993); S. Jin, T. H. Tiefel, M. McCormack, R. A. Fastnacht, R. Ramesh, and L. H. Chen, Science **264**, 413 (1994); P. Schiffer, A. P. Ramirez, W. Bao, and S.-W. Cheong, Phys. Rev. Lett. **75**, 3336 (1995); A. Urushibara, Y. Moritomo, T. Arima, A. Asamitsu, G. Kido, and Y. Tokura, Phys. Rev. B **51**, 14103 (1995).

[3] E. Dagotto, T. Hotta, and A. Moreo, Phys. Rep. **344**, 1 (2001); E. Dagotto, New J. Phys. **7**, 67 (2005).

[4] E. Dagotto, *Nanoscale Phase Separation and Colossal Magnetoresistance*, Springer Series in Solid State Sciences, Vol. 136 (Springer-Verlag, Heidelberg, 2003).

[5] A. Weisse and H. Fehske, New J. Phys. **6**, 158 (2004); A. Weisse, J. Loos, and H. Fehske, Phys. Rev. B **64**, 054406 (2001); **64**, 104413 (2001); **68**, 024402 (2003).

[6] C. Zener, Phys. Rev. **82**, 403 (1951).

[7] Y. Moritomo, Y. Tomioka, A. Asamitsu, Y. Tokura, and Y. Matsui, Phys. Rev. B **51**, 3297 (1995).

[8] D. Senff, P. Reutler, M. Braden, O. Friedt, D. Bruns, A. Cousson, F. Bouree, M. Merz, B. Büchner, and A. Revcolevschi, Phys. Rev. B **71**, 024425 (2005).

[9] B. J. Sternlieb, J. P. Hill, U. C. Wildgruber, G. M. Luke, B. Nachumi, Y. Moritomo, and Y. Tokura, Phys. Rev. Lett. **76**, 2169 (1996).

[10] S. Larochelle, A. Mehta, L. Lu, P. K. Mang, O. P. Vajk, N. Kaneko, J. W. Lynn, L. Zhou, and M. Greven, Phys. Rev. B **71**, 024435 (2005).

[11] M. Medarde, J. F. Mitchell, J. E. Millburn, S. Short, and J. D. Jorgensen, Phys. Rev. Lett. **83**, 1223 (1999); M. Kubota, H. Fujioka, K. Hirota, K. Ohoyama, Y. Moritomo, H. Yoshizawa, and Y. Endoh, J. Phys. Soc. Jpn. **69**, 1606 (2000); X. Qui, S. Billinge, C. Kmety, and J. Mitchell, J. Phys. Chem. Solids **65**, 1423 (2004).

[12] C. D. Ling, J. E. Millburn, J. F. Mitchell, D. N. Argyriou, J. Linton, and H. N. Bordallo, Phys. Rev. B **62**, 15096 (2000).

[13] A. Koizumi, S. Miyaki, Y. Kakutani, H. Koizumi, N. Hiraoka, K. Makoshi, N. Sakai, K. Hirota, and Y. Murakami, Phys. Rev. Lett. **86**, 5589 (2001).

[14] R. Maezono and N. Nagaosa, Phys. Rev. B **61**, 1825 (2000); S. Okamoto, S. Ishihara, and S. Maekawa, *ibid.* **63**, 104401 (2001); G. Jackeli and N. B. Perkins, *ibid.* **65**, 212402 (2002).

[15] A. M. Oleś and L. F. Feiner, Phys. Rev. B **67**, 092407 (2003).

[16] K. Yamamoto, T. Kimura, T. Ishikawa, and T. Katsufuji, and Y. Tokura, Phys. Rev. B **61**, 14706 (2000).

[17] T. G. Perring, D. T. Adroja, G. Chaboussant, G. Aeppli, T. Kimura, and Y. Tokura, Phys. Rev. Lett. **87**, 217201 (2001); K. Hirota, S. Ishihara, H. Fujioka, M. Kubota, H. Yoshizawa, Y. Moritomo, Y. Endoh, and S. Maekawa, Phys. Rev. B **65**, 064414 (2002).

[18] Y. Murakami, H. Kawada, H. Kawata, M. Tanaka, T. Arima, Y. Moritomo, and Y. Tokura, Phys. Rev. Lett. **80**, 1932 (1998); T. Ogasawara, T. Kimura, T. Ishikawa, M. Kuwata-Gonokami, and

Y. Tokura, Phys. Rev. B **63**, 113105 (2001); D. Senff, F. Krueger, S. Scheidl, M. Benomar, Y. Sidis, F. Demmel, and M. Braden, cond-mat/0512305 (unpublished).
[19] T. A. W. Beale, P. D. Spencer, P. D. Hatton, S. B. Wilkins, M. v. Zimmerman, S. D. Brown, D. Prabhakaran, and A. T. Boothroyd, Phys. Rev. B **72**, 064432 (2005).
[20] M. Daghofer, A. M. Oleś, and W. von der Linden, Phys. Rev. B **70**, 184430 (2004); Phys. Status Solidi B **242**, 311 (2005).
[21] L. F. Feiner and A. M. Oleś, Phys. Rev. B **71**, 144422 (2005).
[22] T. Hotta, M. Moraghebi, A. Feiguin, A. Moreo, S. Yunoki, and E. Dagotto, Phys. Rev. Lett. **90**, 247203 (2003).
[23] T. Hotta, Phys. Rev. B **67**, 104428 (2003).
[24] M. Cuoco, C. Noce, and A. M. Oleś, Phys. Rev. B **66**, 094427 (2002).
[25] J. Bała and P. Horsch, Phys. Rev. B **72**, 012404 (2005).
[26] J. van den Brink, G. Khaliullin, and D. I. Khomskii, Phys. Rev. Lett. **83**, 5118 (1999); I. V. Solovyev, Phys. Rev. B **63**, 174406 (2001).
[27] W. Koller, A. Prüll, H. G. Evertz, and W. von der Linden, Phys. Rev. B **66**, 144425 (2002); **67**, 104432 (2003).
[28] A. M. Oleś, Phys. Rev. B **28**, 327 (1983).
[29] A. M. Oleś, G. Khaliullin, P. Horsch, and L. F. Feiner, Phys. Rev. B **72**, 214431 (2005); A. M. Oleś, L. F. Feiner, P. Horsch, and G. Khaliullin, Phys. Status Solidi B **243**, 89 (2006).
[30] K. A. Chao, J. Spałek, and A. M. Oleś, J. Phys. C **10**, L271 (1977); Phys. Rev. B **18**, 3453 (1978).
[31] J. Zaanen and G. A. Sawatzky, J. Solid State Chem. **88**, 8 (1990); A. E. Bocquet, T. Mizokawa, T. Saitoh, H. Namatame, and A. Fujimori, Phys. Rev. B **46**, 3771 (1992).
[32] L. F. Feiner and A. M. Oleś, Phys. Rev. B **59**, 3295 (1999).
[33] J. S. Griffith, *The Theory of Transition Metal Ions* (Cambridge University Press, Cambridge, England, 1971).
[34] A. M. Oleś and L. F. Feiner, Phys. Rev. B **65**, 052414 (2002).
[35] J. van den Brink and D. I. Khomskii, Phys. Rev. Lett. **82**, 1016 (1999).
[36] F. Mack and P. Horsch, Phys. Rev. Lett. **82**, 3160 (1999).
[37] J. van den Brink, P. Horsch, F. Mack, and A. M. Oleś, Phys. Rev. B **59**, 6795 (1999).
[38] S. Yunoki, J. Hu, A. L. Malvezzi, A. Moreo, N. Furukawa, and E. Dagotto, Phys. Rev. Lett. **80**, 845 (1998); E. Dagotto, S. Yunoki, A. L. Malvezzi, A. Moreo, J. Hu, S. Capponi, D. Poilblanc, and N. Furukawa, Phys. Rev. B **58**, 6414 (1998).
[39] K. Hukushima and K. Nemoto, J. Phys. Soc. Jpn. **65**, 1604 (1996); M. C. Tesi, E. J. Janse van Rensburg, E. Orlandini, and S. G. Whittington, J. Stat. Phys. **82**, 155 (1996); K. Hukushima, H. Takayama, and K. Nemoto, Int. J. Mod. Phys. C **7**, 337 (1996); E. Marinari, in *Advances in Computer Simulation*, edited by J. Kertesz and I. Kondor (Springer-Verlag, Berlin, 1997).
[40] In reality, only $J' > 0$ superexchange is allowed due to the charge excitations by t_{2g} electrons between the Mn ions in high-spin states.
[41] D. R. Neuber, M. Daghofer, A. M. Oleś, and W. von der Linden, Phys. Status Solidi C **3**, 32 (2006).
[42] J. B. Goodenough, *Magnetism and the Chemical Bond* (Interscience, New York, 1963); J. Kanamori, J. Phys. Chem. Solids **10**, 87 (1959).
[43] T. Kimura, S. Ishihara, H. Shintani, T. Arima, K. T. Takahashi, K. Ishizaka, and Y. Tokura, Phys. Rev. B **68**, 060403(R) (2003).
[44] J. Salafranca and L. Brey, Phys. Rev. B **73**, 024422 (2006).
[45] M. Daghofer, D. R. Neuber, A. M. Oleś, and W. von der Linden, Phys. Status Solidi B **243**, 277 (2006).
[46] J. Bała, P. Horsch, and F. Mack, Phys. Rev. B **69**, 094415 (2004).
[47] D. Neuber, M. Daghofer, H. G. Evertz, W. von der Linden, and R. M. Noack, Phys. Rev. B **73**, 014401 (2006).
[48] S.-Q. Shen, Phys. Rev. Lett. **86**, 5842 (2001).
[49] J. van den Brink, G. Khaliullin, and D. Khomskii, Phys. Rev. Lett. **86**, 5843 (2001).
[50] The same argument holds for FM chains along the $(\bar{1}1)$ direction.
[51] D. J. Huang, W. B. Wu, G. Y. Guo, H.-J. Lin, T. Y. Hou, C. F. Chang, C. T. Chen, A. Fujimori, T. Kimura, H. B. Huang, A. Tanaka, and T. Jo, Phys. Rev. Lett. **92**, 087202 (2004).
[52] S. B. Wilkins, P. D. Spencer, P. D. Hatton, S. P. Collins, M. D. Roper, D. Prabhakaran, and A. T. Boothroyd, Phys. Rev. Lett. **91**, 167205 (2003); S. B. Wilkins, N. Stojic, T. A. W. Beale, N. Binggeli, C. W. M. Castleton, P. Bencok, D. Prabhakaran, A. T. Boothroyd, P. D. Hatton, and M. Altarelli, Phys. Rev. B **71**, 245102 (2005).
[53] S. S. Dhesi, A. Mirone, C. De Nadaï, P. Ohresser, P. Bencok, N. B. Brookes, P. Reutler, A. Revcolevschi, A. Tagliaferri, O. Toulemonde, and G. van der Laan, Phys. Rev. Lett. **92**, 056403 (2004).
[54] T. Ogasawara, T. Kimura, T. Ishikawa, M. Kuwata-Gonokami, and Y. Tokura, Phys. Rev. B **63**, 113105 (2001).
[55] J. Herrero-Martín, J. García, G. Subías, J. Blasco, and M. C. Sánchez, Phys. Rev. B **72**, 085106 (2005); E. E. Rodriguez, Th. Proffen, A. Llobet, J. J. Rhyne, and J. F. Mitchell, *ibid.* **71**, 104430 (2005).
[56] H. Aliaga, D. Magnoux, A. Moreo, D. Poilblanc, S. Yunoki, and E. Dagotto, Phys. Rev. B **68**, 104405 (2003).
[57] P. Mahadevan, K. Terakura, and D. D. Sarma, Phys. Rev. Lett. **87**, 066404 (2001).
[58] K. Ebata, T. Mizokawa, and A. Fujimori, Phys. Rev. B **72**, 233104 (2005).
[59] As long as the FM chains in the *ab* planes are geometrically oriented as shown in Fig. 12(b).
[60] T. Kimura, K. Hatsuda, Y. Ueno, R. Kajimoto, H. Mochizuki, H. Yoshizawa, T. Nagai, Y. Matsui, A. Yamazaki, and Y. Tokura, Phys. Rev. B **65**, 020407(R) (2002).
[61] G. Kotliar and A. E. Ruckenstein, Phys. Rev. Lett. **57**, 1362 (1986).